Seventeen Million Years of Volcanism Recorded Within the South Hawaiian Seamount Province: Implications for Tectonic Drivers of Intraplate Volcanism

Brandon C Scott[1] and Kevin Konrad[2]

[1]University of Nevada, Las Vegas
[2]Oregon State University College of Earth Ocean and Atmospheric Sciences

August 24, 2024

Abstract

Upwelling and decompression of mantle plumes is the primary mechanism for large volumes of intraplate volcanism; however, many seamounts do not correlate spatially, temporally, or geochemically with plumes. One region of enigmatic volcanism in the ocean basins that is not clearly attributable to plume-derived magmatism are the Geologist Seamounts and the wider South Hawaiian Seamount Province (19°N, 157°W). Here we present new bathymetric maps as well as 40Ar/39Ar age determinations and major and trace element geochemistry for six remote-operated vehicle recovered igneous rock samples (NOAA-OER EX1504L3) and two dredged samples (KK840824-02) from the Geologist Seamounts. The new ages indicate volcanism was active from 90–87 Ma and 74–73 Ma, inferring that, in conjunction with previous ages of ˜84 Ma, seamount emplacement initiated near the paleo Pacific-Farallon spreading ridge and volcanism continued for at least ˜17 m.y. Geochemical analyses indicate that Geologist Seamounts lava flows are highly alkalic and represent low-degree partial mantle melts primarily formed from a mixture of melting within the garnet and spinel stability field. The ages and morphology infer the seamounts were likely not related to an extinct plume. Instead, we build upon previous models that local microblock formation corresponded with regional lithospheric extension. We propose the microblock was bounded by the Molokai and short-lived Kana Keoki fracture zones. Regional deformation and corresponding volcanism among the Geologist Seamounts associated with the microblock potentially occurred in pulses contemporaneous to independently constrained changes in Pacific Plate motion —indicating that major changes in plate vectors can generate intraplate volcanism.

Hosted file

`Scott24 - Geologist SMTs Manuscript.docx` available at https://authorea.com/users/816510/articles/1217177-seventeen-million-years-of-volcanism-recorded-within-the-south-hawaiian-seamount-province-implications-for-tectonic-drivers-of-intraplate-volcanism

Hosted file

`Scott24 - Geologist SMTs Supplemental Document.docx` available at https://authorea.com/users/816510/articles/1217177-seventeen-million-years-of-volcanism-recorded-within-the-south-hawaiian-seamount-province-implications-for-tectonic-drivers-of-intraplate-volcanism

Seventeen Million Years of Volcanism Recorded Within the South Hawaiian Seamount Province: Implications for Tectonic Drivers of Intraplate Volcanism

Brandon Scott[1], Kevin Konrad[1*]

1. Department of Geoscience, University of Nevada Las Vegas, Las Vegas, Nevada 89154, USA

*Corresponding author. Now At Oregon State University. Email: Kevin.Konrad@oregonstate.edu

Highlights

-Volcanic episodes within the Geologist Seamount clusters range from 90 to 73 Ma

-Each volcanic episode has distinct seamount morphology

-Pulses of deformation of young oceanic lithosphere appear to be the best fit for the origin of the volcanism

Abstract

Upwelling and decompression of mantle plumes is the primary mechanism for large volumes of intraplate volcanism; however, many seamounts do not correlate spatially, temporally, or geochemically with plumes. One region of enigmatic volcanism in the ocean basins that is not clearly attributable to plume-derived magmatism are the Geologist Seamounts and the wider South Hawaiian Seamount Province (∼19°N, 157°W). Here we present new bathymetric maps as well as $^{40}Ar/^{39}Ar$ age determinations and major and trace element geochemistry for six remote-operated vehicle recovered igneous rock samples (NOAA-OER EX1504L3) and two dredged samples (KK840824-02) from the Geologist Seamounts. The new ages indicate volcanism was active from 90–87 Ma and 74–73 Ma, inferring that, in conjunction with previous ages of ~84 Ma, seamount emplacement initiated near the paleo Pacific-Farallon spreading ridge and volcanism continued for at least ~17 m.y. Geochemical analyses indicate that Geologist Seamounts lava flows are highly alkalic and represent low-degree partial mantle melts primarily formed from a mixture of melting within the garnet and spinel stability field. The ages and morphology infer the seamounts were likely not related to an extinct plume. Instead, we build upon previous models that local microblock formation corresponded with regional lithospheric extension. We propose the microblock was bounded by the Molokai and short-lived Kana Keoki fracture zones. Regional deformation and corresponding volcanism among the Geologist Seamounts associated with the microblock potentially occurred in pulses contemporaneous to independently constrained changes in Pacific Plate motion —indicating that major changes in plate vectors can generate intraplate volcanism.

Plain Language Summary

Seamounts are volcanic structures on the seafloor that do not breach the surface of the ocean. Most large (e.g. >3 km tall) seamounts are generated from mantle plumes, which are buoyant 'blobs' of anomalously hot mantle that are derived from deep in Earth's interior. These mantle plumes tend to be fixed in their geographic position relative to the mobile lithosphere, ultimately resulting in chains of age-progressive volcanoes (e.g. Hawaiian Islands). However, many seamounts within the ocean basins are not consistent with mantle plume related characteristics like age-progressions. Here we provide new eruption age and chemistry information for volcanics situated within the Geologists Seamount Cluster. The Geologist Seamount Cluster is a group of Cretaceous aged seamounts south of the Hawaiian Islands, within the U.S. exclusive economic zone. The lava flows range in age from 90 to 73 Ma, indicating that at least seventeen million years of volcanic activity occurred in the region. The best model to explain the origin of this volcanism is thinning of the oceanic lithosphere, which causes hot mantle to ascend and melt, while the structure of the nearby divergent plate boundary (ancient Pacific-Farallon Ridge) was being reconfigured.

1. Introduction

The Pacific Basin contains thousands of seamounts of known and unknown geodynamic origins. Seamounts were traditionally defined as rising at least one km above the surrounding seafloor (Menard, 1964); however, modern mapping techniques (e.g. multibeam bathymetry, vertical gravity gradients, satellite altimetry) have revealed that the majority of seamounts are often smaller than one km and most often form near or on spreading ridges, where the lithosphere is young and thin (e.g. Hillier and Watts, 2007, Gevorgian et al., 2023). The largest seamounts (height >3 km) are most often attributed to mantle hotspot processes and can form on old, thick lithosphere distant from any spreading ridge (e.g. Hawaii, Marquesas) or on thin lithosphere near/on a spreading ridge (e.g. Easter, Galapagos) (Hillier and Watts, 2007). The overall number and distribution of seamounts is largely dependent on available ship-track multibeam seafloor mapping. Unfortunately, multibeam data is currently limited with only ~18 % of the Earth's seafloor mapped (Mayer et al., 2018). Nonetheless, modeling with available seafloor data and satellite altimetry has established that there are likely to be >40,000 seamounts with heights >0.5 km (Hillier and Watts, 2007, Gevorgian et al., 2023). The sheer breadth of these seafloor features highlights the potency and longevity of the geodynamic processes that can source submarine volcanism.

Investigation into seamounts that stem from intraplate volcanism—that is volcanism occurring far from plate boundaries—presents an opportunity to deconvolve processes associated with mantle compositional heterogeneities and melting dynamics. Upwelling and decompression of thermochemically anomalous mantle plumes is the primary mechanism for significant intraplate volcanism (Koppers et al., 2021); however, many seamounts dotted across the Pacific Plate do not correlate spatially, temporally, or geochemically with mantle plume volcanism (e.g. Janney et al., 2000, Castillo et al., 2010). Mantle plumes are relatively stationary melt sources that generate sequences of seamounts aligned temporally and spatially with plate motion (e.g. Koppers and Watts, 2010; Wessel and Kroenke, 2008) and entrain a mixture of primitive mantle and recycled lithospheric lithologies and associated geochemical signatures (Hofmann, 2004). The other two prominent mechanisms for intraplate volcanism include lithospheric extension (Sandwell et al., 1995) and asthenospheric shear-driven upwelling (Conrad et al., 2010). Lithospheric extension-derived volcanism involves the thinning of the lithosphere, which in turn can drive adiabatic decompression and partial melting of the mantle (McKenzie and Bickle, 1998). Extension related volcanism is speculated to be generated by a variety of tectonic drivers in the ocean basin, most commonly slab pull from subduction processes (Sandwell et al., 1995; Mather et al., 2020) or by local microplate formation (Sager and Pringle, 1987). Asthenospheric shear-driven upwelling is generated by shear of viscous, fertile fingers in the asthenosphere. The shear is generated by oppositely moving lithosphere and asthenosphere that is able to sustain upwelling mantle (that melts via decompression) at the apex of the finger and downwelling at its rear (Conrad et al., 2010; Ballmer et al., 2013). Age progressions observed among hypothesized shear-driven seamount chains is much faster (e.g. 20–30 cm a^{-1}) than typical absolute plate motion (~7 cm a^{-1} in the Pacific) and seamounts tend to become younger towards the paleo-ridge axis instead of in the direction of absolute plate motion (Ballmer et al., 2013).

Deconvolving intraplate mantle processes requires investigating unique and diverse volcanic structures on the seafloor. The Geologist Seamounts are one such structure located near the Hawaiian Islands, within a region known as the South Hawaiian Seamount Province, that remain understudied (Figures 1, 2). Despite their prominence and proximity to Hawaii, there are only two known attempts to understand Geologist Seamounts' origin through lava flow age determinations (Dymond and Windom, 1964; Sager and Pringle, 1987). Since that pioneering work there has been significant collection of high resolution multibeam bathymetry data that cover nearly the entirety of the seamount chain (a large contributor being the USGS 1986–1989 GLORIA project; Holcomb and Robinson, 2004). Additional rock samples were recovered from the region by the University of Hawai'i-Mānoa School of Ocean and Earth Science and Technology (SOEST) in 1984 and by the National Oceanic and Atmospheric Administration's office of Ocean Exploration Research (NOAA-OE) in 2015. This makes the Geologist Seamounts one of the most surveyed seamount provinces in the Pacific Basin despite the limited studies that utilize the wide breadth of data available for the region.

This work presents new incremental heating $^{40}Ar/^{39}Ar$ age determinations for lava flows recovered from the Geologist Seamounts as well as whole rock major and trace element concentrations and geomorphic analysis of the region using new multibeam bathymetry data. This data is used in conjunction with previous work (Dymond and Windom, 1968; Sager and Pringle, 1987) and plate reconstruction models (Wessel and Kroenke, 2008; Doubrovine et al., 2012; Müller et al., 2019) to constrain the melt mechanisms and sources that generated the Geologist Seamounts.

2. Geologic Setting

2.1 Regional Tectonic Setting

The Geologist Seamounts are located on Pacific crust bounded by the Molokai and Clarion fracture zones (FZ) to the north and south, respectively (Figures 1 and 2). Fracture zones are aseismic, single or multi-strand, remnants of transform faults that offset mid-ocean ridge segments (e.g. Menard, 1967). The most prominent FZs can be traced back millions of years potentially to a still active mid-ocean ridge from which they originated. Moreover, FZs are capable of recording and providing insight into important geodynamic processes including plate reorganization events and microblock formation (e.g. Atwater et al., 1993, Tebbens et al., 1997). In particular, the Molokai and Clarion FZs are 110 Ma, >5,000 km long tracers of transform faults that offset the paleo Pacific-Farallon spreading center (Figure 1). Other prominent Pacific seafloor features proximal to the Geologist Seamounts include the Hawaiian Ridge and the Musician Seamounts to the north, the Mid-Pacific Mountains and the Line Islands to the west, and the South Hawaiian Seamount Province that hosts the Geologist Seamounts (Figure 1, 2).

Here we define the South Hawaiian Seamount Province to be the myriad of seamounts located south of the Hawaiian Islands and east of the Line Islands between the Molokai and Clarion FZs (Figure 2). This includes the Geologist Seamount cluster as well as numerous poorly sampled and sparsely mapped seamounts dotted across the seafloor. Direct sampling and age determinations of the seamounts in the region is lacking. With the exception of the Geologist Seamounts, only one seamount in particular, HD-1 (Figure 2), was sampled and dated unreliably with K-Ar ages ranging from 89–40 Ma from different mineral separates from the same lava flow by Dymond and Windom (1968). However, inferred late Cretaceous ages by paleomagnetic inversion for seamounts HD-1, HD-4, Finch, and the Geologist Seamounts were established by Sager and Pringle (1987).

The southeastern portion of the South Hawaiian Seamount Province consists of Daly Seamount, Finch Seamount, and a series of unexplored smaller volcanic cones that appear to intersect the initiation of the Kana Keoki FZ to the southeast (Figure 3). This E-W trending FZ is relatively short-lived, having existed between ~90 and 70 Ma based on available seafloor age models (Atwater and Severinghaus, 1989; Seton et al., 2020), and has an approximate length of at least 800 km, although mulitbeam mapping of the FZ is sparse. Atwater and Severinghaus (1989) interpreted the FZ as extending eastward into a failed rift that is approximately 550 km long and trending ~N55° (Figure 4). This extension is based on small magnetic isochron offsets at C33n, C32n, and C31n (79.90–69.27 Ma; Ogg, 2020). The Kana Keoki FZ was first observed by Handschumacher and Andrews (1975), however the authors did not speculate on its geologic origin. Sager and Pringle (1987) also mention the Kana Keoki FZ as evidence for Pacific-Farallon spreading ridge reorganization.

Approximately 110 km to the east of the Geologist Seamounts exists a prominent NW-SE trending fault scarp that displays approximately 500 m of offset, coined the Farnella Escarpment by Holcomb and Robinson (2004) (Figure 3). The 180 km long escarpment may intersect the initiation of the Kana Keoki FZ; however, its visible extent ends 190 km away from the FZ. Interestingly, the Farnella Escarpment is not oriented perpendicular to Cretaceous seafloor spreading. Cretaceous seafloor spreading direction in the region is indicated by two sets of abyssal hill fabrics: NNW-SSE (~N345°, west and north of the Geologist Seamounts) and N-S (~N0°, east of the Geologist Seamounts), which are formed from normal faults parallel to the paleo-ridge axis (Figure 4; Holcomb and Robinson, 2004). Currently, no hypotheses have been put forth to explain the origin of this offset but its proximity to the Geologist Seamounts infers a potential related origin.

2.2 The Geologist Seamounts

The Geologist Seamounts are a cluster of ten seamounts located in the North Central Pacific, ~100 km south of the Hawaiian Islands (Figures 1-4). The cluster is easily identified by its inverted V-shape, which is unique to the region. Due to their proximity to the modern Hawaiian Ridge, the seafloor depths of the Geologist Seamounts are modeled to be buoyed ~1 km by the Hawaiian Arc mid-plate swell (Constable and Heinson, 2004). The Geologist Seamounts are located on oceanic lithosphere generated during the Cretaceous Paleomagnetic Quiet Zone Superchron (121-84 Ma; Gradstein et al., 1994), but modeled seafloor ages indicate a ~96–93 Ma age for lithosphere formation (model based on the predicated seafloor half-spreading rates in Seton et al. (2020) as the seamounts reside ~800 km west of the first appearance of C34n (83.65 Ma; Atwater and Severinghaus, 1989). Available K-Ar and $^{40}Ar/^{39}Ar$ age determinations indicate volcanism occurred between 85-79 Ma (Dymond and Windom, 1968; Sager and Pringle, 1987). Thus, the seamounts erupted in an intraplate setting but relatively close to the paleo-ridge axis.

2.3 Petrology and Age Determinations of Geologist Seamounts Lava Flows

Petrologic analysis completed by Friesen (1987) based on rocks dredged from one seamount within the Geologist cluster (Cross Seamount, Figure 3) during the Midpac 2A expedition in 1984 reveals evolved alkaline basalts, biogenic sedimentary rocks, and volcaniclastics. These rocks were dredged along the base and up to the flat-topped summit of Cross Seamount. The major element geochemistry of three recovered igneous rocks from Cross reveal them to be a trachyte, a tephriphonolite, and a basaltic trachyandesite, respectively. Rock names are based on the total alkali versus silica classification scheme (Le Bas, 1986). The igneous rocks fall on the trachytic trend: alkaline-rich with varying silica content. Alteration is abundant and includes pervasive recrystallization of olivine to iddingsite, zeolitization, phosphatization, and oxidation (Friesen, 1987). Also recovered during Midpac 2A was an abundance of volcaniclastics including basaltic hyaloclastite and debris breccia with sedimentary and igneous clasts. This is a common feature on seamounts as volcanism tends to become more explosive when near the ocean surface due to increased volatile (water) influx to the magma system and decreased hydrostatic pressure (Wright and Rothery, 1998). Cross Seamount was once shallow enough for biotic reef formation as evidenced by the recovery of foraminiferal calcarenite and phosphorite from shallow depths (Freisen, 1987), and the fact that it is flat-topped, which is likely caused by wave erosion during subsidence (e.g. Darwin, 1842; Hess, 1946; Smoot, 1995). Dymond and Windom (1968) also recovered three igneous rocks from Cross Seamount of which they classified all as trachytes but did not provide geochemical data. Sager and Pringle (1987) and Pringle (1992) analyzed a trachyte from McCall and a trachyte and hawaiite from Cross, and provide whole rock and plagioclase K, Rb, Sr, Sm, and Nd trace element data.

Available age determinations from the Geologist Seamounts are limited to two seamounts. Prior to this work, K-Ar and $^{40}Ar/^{39}Ar$ total fusion age determinations were obtained from igneous rocks recovered from McCall and Cross Seamount (Dymond and Windom, 1968; Sager and Pringle, 1987). The K-Ar age determination experiments utilized biotite and whole-rock trachyte separates, which range from 78.8 to 85.5 Ma (Dymond and Windom, 1968). K-Ar analysis on biotite phenocrysts of Sample 7-12 (85.5 ± 4.0 Ma, 2σ) and on a whole-rock separate from the same lava flow (78.8 ± 3.4 Ma, 2σ) contained substantial error. The large uncertainties, coupled with the general assessment that K-Ar age determinations on seawater altered lava flows fail to accurately represent the age of eruption (e.g. Pringle, 1992) indicate the ages should not be used in regional interpretations. Sager and Pringle (1987) and Pringle (1992) provide $^{40}Ar/^{39}Ar$ total fusion analysis on lava flow separates from McCall and Cross. $^{40}Ar/^{39}Ar$ total fusion analyses is a method that is akin to K-Ar, wherein the sample is irradiated to convert ^{39}K to ^{39}Ar but the gas is released and analyzed from the whole rock or mineral separate in one high temperature fusion step. Sager and Pringle (1987) assigned eruption ages of 84 ± 1 Ma (2σ) to the McCall seamount based on three analyses (two plagioclase separates and a trachyte; recalculated to the same fluence monitor, age and decay rate used in §3.1) and 85 ± 8 (2σ) Ma to Cross guyot based on three analyses (biotite from Dymond and Windom (1968), a trachyte, and a hawaiite).

3. Materials and Methods

3.1 $^{40}Ar/^{39}Ar$ Age Determination Methodology

During NOAA-OE expedition EX1504L3 in 2015, eight lava flow samples were collected from three seamounts (McCall, Swordfish, and Ellis) among the Geologist Seamount cluster by ROV *Deep Discoverer*. Additionally, four lava flow samples were dredged from two seamounts (Cook and Jaggar) during SOEST expedition KK840824-02 in 1984 but never analyzed. Of the twelve igneous samples, eight were chosen for incremental heating age determination experiments. These include seven plagioclase-rich alkaline basalts and one phosphorite-cemented conglomerate with a pebble-sized (~40mm) fresh alkaline basalt clast. This sample suite covers eruptions from five of the ten Geologist Seamounts. Plagioclase, amphibole, and holocrystalline groundmass were the target phases for $^{40}Ar/^{39}Ar$ age determinations for the eight lava flow samples. Selection of the target phases was based on petrographic observations of each sample with a focus on minimizing effects from secondary alteration.

Sample preparation began with the removal of altered sections and ferromanganese crust from the bulk rock through cutting with a diamond-blade trim saw. Bulk rock was reduced in size in a BICO steel jaw chipmunk crusher followed by grinding in a BICO rotary disk mill. Sufficient material for analysis was produced by alternating grinding and sieving to reach a specific size based on desired phase: 250–500 µm for plagioclase (targeting ~20 mg) and amphibole (~10 mg); 212–300 µm for groundmass (~20 mg). These fractions were sonicated with ultrapure water at room temperature to remove rock powder produced during grinding and were dried in a 50°C drying oven for 24–48 hours. Concentration of the desired phase was achieved with a Frantz isodynamic magnetic separator. Since secondary alteration was generally abundant, acid leaching was incorporated to remove clay and carbonate. Separates were acid leached using an ultrasonic bath heated to approximately 40°C for sixty minutes each in 3N HCl, 6N HCl, 1N HNO3, and 3N HNO3 sequentially, followed by a heated ultrapure water bath (Konrad et al., 2018). Plagioclase separates underwent an additional bath (prior to ultrapure water) in 4% HF for 10–15 minutes to remove potential sericite rims. Separates were hand-picked under a microscope with careful avoidance of non-targeted minerals, surface alteration, and inclusions. Separates were packed into aluminum foil and placed into quartz tubes with accompanying standards of known fluence age (Fish Canyon Tuff sanidine). Samples were then irradiated in Oregon State University's TRIGA Reactor for nine hours.

Analyses were conducted with the incremental heating method using a double-vacuum furnace attached to a stainless-steel extraction line at the Nevada Isotope Geochronology Laboratory (NIGL). Gases were exposed to a hot SAES 'getter' during fourteen minutes of furnace heating followed by an additional six-minute exposure to a second set of room temperature and hot SAES 'getters'. Processed gas was inlet into a NGX multi-collector noble gas mass spectrometer with ATONA amplifiers with time zero initiated after a 20s gas equilibration time. Argon isotopic ratios were measured in a NGX multi-collector mass spectrometer following procedures outlined in Balbas et al. (2023). Age determinations were calculated using ArArCalc software (Koppers, 2002) with the propagated uncertainties described in Balbas et al. (2023). Ages were calculated against a Fish Canyon Tuff sanidine fluence monitor with an assumed age of 28.201 ± 0.08 Ma (Kuiper et al., 2008) and using a ^{40}K total decay constant of 5.463 ± 0.107×10^{-10} yr^{-1} (Min et al., 2000).

3.2 Major and trace element geochemistry methodology

Seven bulk rock samples were cut into small, ~20–80g pucks for geochemical analyses. Secondary mineralization veins, highly altered areas, and particularly phenocryst-rich sections were avoided to prevent concentrating specific phases and creating bias in the data. Pucks were polished with Al grit to remove saw marks. Then pucks were repeatedly sonicated in deionized water to remove any residual Al grit. Cleaned pucks were sent to the XRF and ICP-MS laboratory of Michigan State University and analyzed in triplicate according to the methods of Rooney et al. (2011; 2015). All major element data presented herein is from XRF while all provided trace element analyses were measured via solution ICP-MS.

4. Results

4.1 Morphology of Seamounts

The Geologist Seamounts have four distinct morphologies: (1) round, flat-topped guyots; (2) conical, radial-topped seamounts; (3) narrow, elongate ridges with steep slopes; and (4) elliptical, elongate seamounts with irregular topography. Of the ten seamounts, one is a guyot, one is an elliptical seamount, three are radial seamounts, and five are elongate ridges. Table 1 describes the location and characteristic features of each seamount. Detailed maps and descriptions of individual seamounts are provided in Supplemental Document 1.

4.2 Descriptions of Volcanic Rocks

An alkalic suite of lavas was recovered from several sites in the Geologist Seamount cluster (see location data in Table 2 and major and trace element data in Table 3). Ferromanganese oxide encrusted all of the recovered samples. Fresh cores persist in the suite of samples although secondary alteration is pervasive to varying degrees. Among our sample set, olivine is always recrystallized to clay iddingsite. Rock names are based on the total alkali versus silica classification scheme (Le Bas, 1986; Figure 14). Hand sample and in-situ images of lava flows are available in Figure 5, and cross-polarized thin section images of lava flows are available in Figure 6.

4.2.1 Swordfish Seamount

Samples recovered from Swordfish include two sparsely porphyritic trachyandesites (EX1504L3-D5-1, Figure 5A; EX1504L3-D5-6, Figure 5C) and a volcanic breccia (EX1504L3-D5-4, Figure 5B). Cross-polarized images are displayed in Figure 6C and Figure 6D. The alkalic samples are highly vesicular with round vesicles that lack infilling. Phenocrystic plagioclase is typically subhedral with common disequilibrium textures and reaction rims of sericite. Rare (~1%) amphibole and clinopyroxene phenocrysts also occur, both displaying subhedral crystal shape and partial recrystallization. Groundmass consists of plagioclase, magnetite, and altered fine-grain mesostasis.

The volcanic breccia is phosphorite-cemented with numerous oxidized basalt clasts and one fairly fresh basalt clast (Figure 5B). The fresh clast is a moderately porphyritic vesicular basalt with common subhedral plagioclase phenocrysts containing disequilibrium textures (Figure 6E). Vesicles are rounded to elongate. Groundmass consists of plagioclase, magnetite, and altered mesostasis.

4.2.2 Ellis Seamount

One sample recovered from Ellis is a basanite (EX1504L3-D6-2, Figure 5D). The basanite is highly vesicular and sparsely phenocrystic (Figure 6F). Vesicles are sub-rounded, partly infilled, and often contain reaction rims. Olivine phenocrysts and microcrysts are anhedral. The groundmass consists of olivine, plagioclase, and altered mesostasis.

4.2.3 Cook Seamount

One sample recovered from Cook is a basanite (KK840824-02 STA76 RD45, Figure 5E). The sample is vesicular, trachytic, and moderately porphyritic with abundant euhedral plagioclase phenocrysts and occasional subhedral olivine phenocrysts (Figure 6G). Vesicles are sub-rounded to elongate and are partially infilled by calcite and phosphorite. Groundmass consists of lath-like plagioclase, olivine, magnetite and mesostasis.

4.2.4 Jaggar Seamount

A phonotephrite (KK840824-02 STA76 RD46, Figure 5F) was recovered from Jaggar. The sample is trachytic, vesicular, and sparsely porphyritic with occasional subhedral plagioclase phenocrysts that often contain disequilibrium textures (Figure 6H). Vesicles are rounded, lack infilling, and have alteration coating. Plagioclase, magnetite, and altered mesostasis comprise the groundmass.

4.2.5 McCall Seamount

A basanite (EX1504L3-D4-4, Figure 5G) and a hawaiite (EX1504L3-D4-1, Figure 5H) were recovered from McCall. The basanite was likely part of a larger volcanic breccia as evidenced by the phosphorite and altered basalt clasts adhered to its rim. Both samples are sparsely porphyritic with rare, large subhedral plagioclase phenocrysts (Figure 6A and Figure 6B). The basanite is trachytic and the hawaiite is vesicular. Vesicles are rounded, have minor infill, and have alteration coating. Occasional plagioclase microcrysts are subhedral. Plagioclase, olivine, spinel, and altered mesostasis makeup the groundmass of both samples.

4.3 Compositions of Volcanic Rocks

4.3.1 Major Elements

Loss on Ignition (LOI) values, which represents the lost volatile content when the sample was heated, are substantial for every sample [1.6–5.6 wt.%] and should be taken into consideration when regarding the validity of the major and trace element data (Table 3). Figure 7 displays major element bivariate diagrams of Geologist Seamount lavas compared to Pacific intraplate extensional lavas (Janney et al., 2000; Davis et al., 2010), mantle-plume derived lavas (Willbold and Stracke, 2006), and spreading-center derived lavas from the East Pacific Rise (EPR; Strake et al., 2022). Overall, MgO content is very low in all of the recovered rocks (<1.50 wt.%) potentially due to secondary alteration, which removes the ability to accurately evaluate differentiation (Figure 7E). There are elevated P_2O_5 values for the Geologist Seamounts lava flows, which range from 1.0–5.0 wt.%. (Figure 7I). Relatively high TiO_2 [1.6–3.0 wt.%], Al_2O_3 [17.1–19.7 wt.%], and Na_2O [3.1–5.4 wt.%] concentrations are present within the Geologist Seamount lava flows, similar to alkaline lavas recovered from other intraplate volcanoes such as the Pukapuka Ridge (e.g. Janney et al., 2000 [TiO_2: 1.4–2.8; Al_2O_3: 16.7–18.1; Na_2O: 3.6–6.4]) or offshore California seamounts (Davis et al., 2010 [TiO_2: 0.6–3.9; Al_2O_3: 15.4–21.0; Na_2O: 2.5–5.8]) (Figure 7A, 7B, 7G).

Based on the total alkali versus silica plot, rocks recovered from the Geologist Seamounts include basanite, phonotephrite, hawaiite (trachybasalt), and trachyandesite (Table 3; Figure 8). The most common rock type is basanite, which are observed on Cook, Ellis, and McCall seamounts. The basanites all plot on the border of the basanite and hawaiite fields, so they are not overly undersaturated in silica (42.6–46.4 wt.%) nor supersaturated in total alkalis (5–6.4 wt.%). McCall seamount contains a hawaiite flow (EX1504L3-D4-1) that displays the lowest K_2O content of all the recovered samples from the region (1.04 wt.%; Figure 7H). The trachyandesite samples come from Swordfish seamount and contain the highest silica (EX1504L3-D5-1: 54.9 wt.%; D5-6: 53.5 wt.%) and total alkali (EX1504L3-D5-1: 9.6 wt.%; D5-6: 9.1 wt.%) content of all recovered samples (Figure 8). Lastly, the lava flow from Jaggar seamount (KK840824-02 STA77 RD46) is a phonotephrite that is near the border of phonotephrite and basaltic trachyandesite fields; therefore, it is not supersaturated in total alkalis (7.9 wt.%; Figure 8). Overall, the lava flows recovered from the Geologist Seamounts fall along the alkaline to highly alkaline compositional trends—consistent with previous observations on the region (Friesen, 1987; Pringle, 1992).

4.3.2 Trace Elements

Whole rock trace element concentrations are provided in Table 3. Due to their resistance to hydrous remobilization during low-temperature seawater alteration, HFSE (high-field strength elements) like Th, Nb, Hf, Zr, Ta and REE (rare earth elements) are the primary trace elements to focus on when working with submarine lava flows (Bienvenu et al., 1990). Samples from Northern McCall ridge (EX1504L3-D4-1 and -4) contain the lowest incompatible trace element concentrations among the Geologist Seamounts samples. The primitive mantle normalized (PM) (McDonough and Sun, 1995) $(La/Sm)_{PM}$ ratios for the Northern McCall lava flows vary from 1.7–2.3, while the other lava flows range from 2.7–3.4 (Figure 9B). However, the total range of $(La/Sm)_{PM}$ for the Geologist seamount samples mostly overlap with alkalic basalts derived from seamounts and ocean islands (Figure 9B). The heavy rare earth elements (HREE) ratios vary among the samples with $(Dy/Yb)_{PM}$ ranging from 1.15–1.76, which reside at the lowest end of most OIB values (e.g. 1.6–2.4; Figure 9B). The Nb/Zr values for the Geologist lava flows range from 0.07–0.22 and coincide with the full range of MORB (~0.009–0.22) and OIB (0.08–0.36) (Figure 9A). With the exception Northern McCall ridge, the Geologist lava flows contain Nb/Yb values (16.4–45.3) consistent with other oceanic alkaline basalts (0.9–44.5), while the McCall ridge samples (0.34 and 6.75) overlap with MORBs (~0.01–12.7; Figure 10A).

The Y/Y* ratio, which is the ratio of primitive mantle normalized Y concentration in the lava flows relative to the expected mantle array ($Y/Y^* = (Y/Y_{PM}) / \sqrt{(Dy/Dy_{PM} * Ho/Ho_{PM})}$), is commonly employed to test for phosphorite contamination as phosphorite preferentially uptakes Y relative to Dy and Ho (Geldmacher et al., 2023). The Y/Y* values in the Geologist Seamounts lava flows range from 0.8–1.15. The observed Y/Y* values indicate minor phosphate contamination in sample EX1504L3-D4-4 (Figure 11), although, there does not appear to be a clear relationship between P_2O_5 enrichment and HREE enrichment in our sample set (R^2 of P_2O_5 vs. La, Sm, or Yb are 0.16, 0.38, and 0.04, respectively). For example, EX1504L3-D4-4 has the highest P_2O_5 value (5.2 wt.%) whilst having no clear relative enrichment in any characteristic REE (e.g. La: lowest at 25.4, Sm: second lowest at 6.9, and Yb: third highest at 4.5).

Figure 12 shows C1 carbonaceous chondrite-normalized (McDonough and Sun, 1995) REE profiles of lava flows from the Geologist Seamounts compared to average end-member ocean island basalt composition (Willbold and Stracke, 2006) and min-max mid-ocean ridge basalt composition (Gale et al., 2013). Geologist Seamounts lavas show a steep slope (enrichment in LREE; light rare earth elements), and high LREE/HREE values with La/Yb values range from 11.8-20.0, excluding EX1504L3-D4-1 [5.8] and D4-4 [5.7]. The most alkali rich flows, trachyandesites from Swordfish (EX1504L3-D5-1; D5-6), have the steepest profiles. The least alkali rich lava flow, the Hawaiite from Northern McCall ridge (EX1504L3-D4-1), has the shallowest profile. Conservatively, we do not use the large ion lithophile element concentrations when assessing our data as they are highly susceptible to low-temperature aqueous remobilization during the lava flows long residence on the seafloor (e.g. Geldmacher et al., 2023). For example, the large ion lithophile elements Ba and Sr have wide-ranging values among our dataset, from ~70–1120 and ~360–1480, respectively (Table 3).

4.4 $^{40}Ar/^{39}Ar$ Age Determinations

Ten $^{40}Ar/^{39}Ar$ experiments of eight igneous rocks produced five concordant age plateaus of reliable data (Figure 13). Here we define a concordant heating plateau as containing >50% of the $^{39}Ar_{(K)}$ released and having a probability of fit factor (P) >0.05. Two plagioclase separates from Northern McCall Seamount, EX1504L3-D4-1 and EX1504L3-D4-4, produced age plateaus of 87.9 ± 0.7 Ma (P = 0.06, MSWD: 2.2, $^{40}Ar/^{36}Ar_{int}$: 286 ± 19, $^{39}Ar_{(K)}$ = 51%) (Figure 13A) and 90.3 ± 0.6 Ma (P = 0.42, MSWD: 1.0, $^{40}Ar/^{36}Ar_{int}$: 302 ± 24, $^{39}Ar_{(K)}$ = 92%) (Figure 13B), respectively. A small amphibole separate (2.0 mg) from Swordfish Seamount, EX1504L3-D5-1, produced an age plateau of 87.3 ± 0.2 Ma (P = 0.99, MSWD: 0.2, $^{40}Ar/^{36}Ar_{int}$: 294 ± 36, $^{39}Ar_{(K)}$ = 96%). Plagioclase separates from Cook and Jaggar Seamounts, KK840824-02 STA76 RD45 and KK840824-02 STA76 RD46, produced concordant age plateaus of 73.9 ± 0.2 Ma (P = 0.37, MSWD: 1.1, $^{40}Ar/^{36}Ar_{int}$: 281 ± 21, $^{39}Ar_{(K)}$ = 100%) and 72.8 ± 0.3 Ma (P = 0.10, MSWD: 1.6, $^{40}Ar/^{36}Ar_{int}$: 329 ± 37, $^{39}Ar_{(K)}$ = 65%), respectively. The other five experiments produced discordant heating spectrums that were marred by significant recoil (Figure 13B, 13H), degassing of low temperature alteration phases (Figure 13H), and instances of excess Ar domains that prevented concordance between incremental heating steps (Figure 13G, 13F)

Of the five analyses that failed to produce a concordant age plateau, three were groundmass separates and two were plagioclase separates. All groundmass samples, EX1504L3-D4-1 (Figure 13B), EX1504L3-D5-1 (Figure 13E), and EX1504L3-D6-2 (Figure 13H) experienced high temperature recoil effects likely stemming from the displacement of $^{39}Ar_{(K)}$ from phases that degas at low temperatures (e.g. glass; clay alteration) into higher temperature phases (e.g. clinopyroxene) or out of the solid system, resulting in low apparent ages. EX1504L3-D4-1 and EX1504L3-D5-1 (groundmass) experienced low temperature partial degassing effects (low apparent ages) mixed with some low temperature recoil (higher apparent ages) that may relate to partial degassing during the emplacement of overlying lava flows and/or degassing of fine grain secondary minerals that crystalized progressively after lava flow emplacement. The discordant plagioclase, EX1504L3-D5-4 (Figure 13F) and EX1504L3-D5-6 (Figure 13G), analyses experienced low temperature degassing of recrystallized plagioclase (sericite) (low apparent ages from loss of $^{40}Ar^*$ and addition of ^{39}K post lava emplacement) and were blighted with multiple excess ^{40}Ar domains, likely from melt inclusions within the crystal separates (resulting in high apparent ages).

5.0 Discussion

New age determinations define the Geologist Seamounts cluster as forming either continuously over ~17 m.y. or during at least three potential episodes of volcanism: 90–87 Ma, 84 Ma, and 74–73 Ma. Lava flows are alkalic (Figure 8) vary from moderately enriched in LREE to highly enriched (e.g. La/Sm_{PM} = ~1.7–3.4) with low to moderately high HREE slopes (e.g. Dy/Yb_{PM} = ~12–18; Figure 9B). Aqueous alteration is pervasive, which creates difficulty in accurately analyzing major element differentiation trends, however most of the HFSE trace element ratios appear reliable. Morphology of the Geologist Seamounts is variable along the cluster and appears to be influenced by local ocean-crustal fabrics (Supplemental Document). Below we discuss the new observations on the Geologist Seamounts in detail and place their origin within the larger tectono-magmatic framework of the Pacific plate.

5.1 The Age and Morphology of the Geologist Seamounts

The new age determinations appear to highlight a first-order relationship between seamount morphology and eruption age among the Geologist Seamounts cluster. A N-S dominant axis orientation is shared by Northern McCall and Swordfish seamounts whose sampled lava flows formed from 90–87 Ma. Due to Geologist Seamount formation on lithosphere created during the Paleomagnetic Quiet Zone Superchron (121-84 Ma; Gradstein et al., 1994), the age of ocean crust is modeled to be ~96–93 Ma based on half-spreading rate of the Pacific Plate (~68 mm a^{-1}) calculated by Seton et al. (2020). McCall and Swordfish seamounts reside 700 km and 850 km from the first occurrence of C34n (83 Ma, Seton et al., 2020), respectively. A local half-spreading rate of 68 mm a^{-1} from Seton et al. (2020) results in a modeled crustal age of 93.3 Ma and 95.5 Ma for the seamounts. Therefore, the new Northern McCall and Swordfish lava flows ages (90–87 Ma) are approximately 3–8 Ma younger than the underlying oceanic crust placing them near the paleo-Pacific-Farallon ridge. The seamount along-axis orientation is aligned with the regional abyssal hill fabric (Figure 4) east of the cluster indicating the seamounts likely formed from fissure eruptions and dike emplacement along the pre-existing N-S normal faults.

Lava flows from the NE-SW orientated central McCall seamount formed at 84 Ma (Sager and Pringle, 1987), which is consistent with its geographic superposition on the northern McCall ridge (Figure S5). A change in preferential channeling of volcanism occurred between the 90–87 Ma and 84 Ma episodes of volcanism. The N-S orientation is shared by abyssal hills east of the Geologist Seamounts and north of the Kana Keoki FZ (Figure 4). The abyssal hills formed at an approximately 15° clockwise offset (oriented ~N0°) from the abyssal hills on Pacific seafloor west and north of the Geologist Seamounts, which are oriented at ~N345°. Clockwise rotation of abyssal hill fabrics may be indicative of microblock formation because they are known to rotate independently (e.g. Mammerickx et al., 1988; Tebbens et al., 1997; Matthews et al., 2016), or more simply, may represent a change in plate motion. Long axis orientations of seamounts in the NE-SW direction is the most common structure among the Geologist Seamounts cluster. Four seamounts have NE-SW orientations within the cluster (Washington, Ellis, Perret, and central McCall). However, there are no local crustal fabrics in this direction besides a distant, proposed rift zone (~18°N, 144°W; Atwater and Severinghaus, 1989) that potentially represents the eastern boundary of an extinct microblock between the Kana Keoki and Molokai FZs (Figure 4) (Discussed further in §5.6).

A third episode of volcanism occurred on Cook and Jaggar seamounts whose two recovered lava flows have eruption ages of 73.9 and 72.8 Ma, respectively (Figure S4 and Figure 13). These lava flows are approximately 20 Ma younger than the underlying oceanic crust and would place the Geologist Seamounts firmly off-ridge at the time. Jaggar is the only seamount-oriented NW-SE, which is shared by the Farnella Escarpment and abyssal hill fabrics west of the Geologist Seamounts cluster. However, this orientation is not ubiquitous across the seamount as it is not an elongate ridge similar to Perret or Ellis and there are distinct volcanic cones dotted across the seamount that call into question whether this seamount originated from a single eruptive pulse at *ca.* 74 Ma (Figure S4), or if there were multiple pulses of volcanism, potentially over millions of years as is seen with McCall seamount. Cook seamount has a radial structure with no preferential orientation, which is also shared by Pensacola and Daly seamounts (Figure S4 and S6). Radial (stellate) seamount structure is expected when volcanic growth radiates from a central peak into several pre-existing crustal weaknesses (Mitchell, 2001; Chaytor et al., 2007). The existence of radial seamounts in close proximity to seamounts with clear orientations suggests that the local stress regimes that generated the Geologist Seamounts were not ubiquitous and/or consistent. In summary, we see a *ca.* 90–87 Ma pulse of volcanism dominantly oriented in the N-S direction, a *ca.* 84 Ma pulse of volcanism oriented in the NE-SW direction, and a *ca.* 74–73 Ma pulse of volcanism with no clear orientation. The lack of consistency across the cluster overtime brings into question of how has the geologic context surrounding the Geologist Seamounts changed during each episode of volcanism and were there any distinct changes in the chemical composition of the lava flows indicating changes in mantle melting and source reservoirs?

5.2 Geochemical Trends

The new trace element concentration data from the Geologist Seamounts aid in illuminating the tectonomagmatic processes that formed the Geologist Seamounts. Due to the presence of significant aqueous alteration among our dataset we restrict interpretations to key HFSE ratios as well as REE behavior. As a whole, the lava flows from the Geologist Seamounts show a wide range of trace element heterogeneity, highlighting significant variation in melting dynamics during seamount emplacement. The patterns of HREE (e.g. Dy/Yb) can be used as indicator of the degree of mantle melting within the garnet stability field (e.g. deeper than ~80 km; Dy/Yb_{PM} values >16) as compared to melting within the shallow spinel stability field (lower Dy/Yb_{PM} values <16). This is due to the tendency for HREEs to remain in the mantle residual garnet due to their increased compatibility in garnet as compared to spinel (e.g. McKenzie and O'Nions, 1991). Mantle plume derived hotspot volcanism (e.g. purple fields Figure 9, 10, and 12), tend to melt deeper in the asthenosphere due to the increased temperature of plumes (e.g. Hoffmann, 2003). In contrast, MORBs represent high degree melting of shallower asthenosphere and thus display low Dy/Yb (~1–15). The La/Sm (a proxy for the slope of the LREEs), is typically reflective of either lower degrees of mantle melting (which increase La/Sm) or melting of more incompatible element enriched mantle reservoirs (also increases La/Sm). In combination, these ratios can provide first order insights into the depth and degree of mantle melting sourcing the lava flows.

The bulk of the analyzed Geologist Seamount lavas show $(Dy/Yb)_{PM}$ that overlap with lowest end of most OIB values and higher end of non-plume related offshore California seamounts (Dy/Yb_{PM} = ~17; Figure 9B), which suggests a mix of melting within the garnet and spinel stability fields. With the exception of Northern McCall ridge, all the Geologist Seamount samples have high La/Sm (>2.7), consistent with their highly alkalic nature. A further way to test for degree of melting of asthenosphere melting is by comparing Nb/Yb to Th/Yb (Figure 10A). Alkaline lavas sourced from low degrees of mantle melting trend towards elevated Nb and Th for a given Yb concentration (Pearce, 2007). The Geologist lava flows plot in the alkalic field (Nb/Yb = ~4–30 and Th/Yb = ~0.3–2.5), overlapping with the compositional fields of Pukapuka Ridge (Nb/Yb = ~0.1–80 and Th/Yb = ~0.05–9; Janney et al., 2000), offshore California seamounts (Nb/Yb = ~10–35 and Th/Yb = ~1–3; Davis et al., 2010) and OIB (Nb/Yb = ~20–50 and Th/Yb = ~0.8–7; Wilson and Stracke, 2006). Importantly, any recycled continental crustal materials in a mantle reservoir (e.g. enriched mantle, EM; Zindler and Hart, 1986) would result in higher Th for a given Nb concentration (trend arrows in Figure 10A; Pearce, 2007). The Geologist Seamounts do not display any evidence of recycled continental or oceanic crust in their trace element compositions.

The two-outlier lava flows from each of the trace element trends are from Northern McCall Ridge (Figure 9, 10; D4; 90 Ma). The ridge hosts the oldest lava flow samples and the eruptions would have occurred near the spreading axis. The two D4 samples are the least alkalic in the suite (total alkali: D4-1 = 5.6 wt. %; D4-4 = 5.5%) excluding D6-2 (total alkali = 5.3 wt. %) and show evidence for higher degrees of shallower mantle melting compared to the other Geologist Seamount lava flows (Figures 9, 10). The higher degrees of melting are consistent with the Northern McCall Ridge lava flows being emplaced on the youngest, hottest and thinnest crust and thus would likely have been an easier setting to generate higher degrees of melting.

The bulk of Geologist Seamount lava flows plot consistently on the overlap between the plume derived OIB fields and extension derived seamount fields (Figures 9, 10). The largest indicator of separation between the two fields is the $(Dy/Yb)_{PM}$ composition, which better overlaps with the California seamounts and indicates shallower melting than typical OIB.

As shown above, REE trends and HFSE behaviors are often utilized in marine basalts to differentiate between magmatic processes (e.g. Janney et al., 2000; Castillo et al., 2010); however, low temperature seawater alteration and phosphatization (in particular) may alter their initial magmatic abundances (Ludden and Thompson, 1979; Bienvenu et al., 1990; Geldmacher et al., 2023). The calculated Y/Y* values are a means for checking for phosphorite contamination and associated REE enrichment (Geldmacher et al., 2023). There appears to be some enrichment of Y in samples D4-4 and D6-2 according to P_2O_5 content (e.g. D4-4: Y/Y* = 1.14 and P_2O_5 = 4.38; D6-2: Y/Y* = 0.92 and P_2O_5 = 3.05), but it is not ubiquitous within this suite of lavas from the Geologist Seamounts (e.g. D4-1: Y/Y* = 0.88 and P_2O_5 = 0.95). Given the high LOI and P_2O_5 for most of the Geologist lava flows, clearly defining whether the flows preferentially overlap with plume or extension derived intraplate volcanoes is not possible.

In summary, the Geologist Seamounts lava flows appear to represent melting within both the garnet and spinel stability fields and represent low-degree melts. The exception to this is the 90 Ma, Northern McCall ridge lava flows. Samples from the ridge (EX1504L3-D4-1; D4-4) appear to represent melting primarily in the spinel-stability field, coupled with higher degrees of melting. These signatures are consistent with the lava flows being emplaced on what would have been the youngest crust during volcanism. Provided that the geochemistry does not provide unambiguous insights, other observations need to be considered when deconvolving the origin of these enigmatic seamounts. Where were the Geologist Seamounts on the Pacific Plate during each episode of volcanism; moreover, do any of the recorded volcanic episodes correspond geographically to regions of active volcanism today (e.g. hotspots)?

5.3 Paleo Reconstruction of Seamounts

Reconstructing and modeling the geographic coordinates of the Geologist Seamounts at the time of formation aids in deciphering their origin and relationship with the paleo mid-ocean ridge and proximal mantle plumes. Hotspotting is a method that utilizes present-day geographic positions of supposedly hotspot related seamounts and seafloor motion paths (e.g. plate motion paths) to reconstruct the location of a relatively fixed hotspot (Wessel and Kroenke, 1997). If we consider a seamount with a determined radiometric age (e.g. Cook Seamount: 74 Ma), then we can assess its latitude and longitude coordinates at the time of eruption to better illuminate whether the seamount's eruptive location correlates to a hotspot anomaly in that area today (e.g. most of the seamounts in the Western Pacific Seamount Province correlate to active hotspots in the SOPITA region today; Konter et al. 2008). Figure 14 displays the paleo location of the Geologist Seamounts from 90 Ma (the first recorded episode of volcanism—yellow diamonds and squares) to 73 Ma (the last recorded episode of volcanism—blue diamonds and squares) based on two plate motion models (Wessel and Kroenke, 2008, diamonds; Doubrovine et al., 2012, squares) overlain on modern-day mantle shear-wave seismic anomaly (in %) at 2700 km depth. Black stars in Figure 14 show the present-day locations of several different hotspots, which are argued to be thermochemical upwellings of deep mantle material that generate at the margins of large low shear velocity provinces at the core-mantle boundary (Burke et al., 2008). One such province is the SOuthern Pacific Isotopic and Thermal Anomaly (SOPITA), which is geographically constrained by the upwelling of thermochemical plumes, which are identified by their slowing effect on shear-wave velocity within the mantle and their unique chemical identity (Staudigel et al., 1991; Hasse et al., 2019). As such, we can compare the Geologist Seamounts' location at the time of eruption to shear velocity anomalies at the core-mantle boundary (~2700 km depth) to justify the plausibility of plume-derived volcanism within the Geologist Seamounts cluster (Figure 14). There is no known mantle plume in the area during three melting episodes (90–87 Ma, 84 Ma, and 74–73 Ma); however, the lithosphere did override a negative shear anomaly province during the 90–87 Ma and 84 Ma episodes of volcanism but not during the 74–73 Ma episode (Figure 14, French and Romanowicz, 2015). Therefore, we cannot fully resolve the likelihood of a mantle plume origin solely based on the eruptive paleo location of the Geologist Seamounts.

5.4 Mantle Plume Origin?

Mantle plumes are thermochemical upwellings of mantle material with a fixed location in relation to the lithosphere (Koppers et al., 2021). Volcanism from mantle plumes generate age-progressive chains of seamounts due to plate motion atop the plume (Morgan, 1971; Wessel and Kroenke, 2008; Koppers et al., 2021). Geologist Seamounts lava compositions have similarities to plume derived OIBs but do not unambiguously support a mantle plume origin (Figures 9, 10, and 11). During the late Cretaceous, the Pacific plate in the Geologist Seamounts region is generally drifting NW with some small shifts in vectors (Koppers et al., 2001; Wessel and Kroenke, 2008). The Geologist Seamounts trend oblique (N-NE) to absolute plate motion (~NW). Moreover, they do not display age progression correlated with plate motion, that is, the 90 Ma lava flows are not in the northwest and progress to younger emplacement ages towards the southeast as would be expected from plume volcanism during the late Cretaceous.

Figure 15A-C represents hypothetical plume motion-paths if the aforementioned three volcanic episodes within the Geologist Seamounts were independently sourced from fixed mantle plumes. Due to the fixed nature of mantle plumes, a seamount chain should form overtime as the plate moves over the plume to generate age-progressive volcanic centers (e.g. The Hawaiian-Emperor seamount chain; Figure 1; Wessel and Kroenke, 1997). This phenomenon is known as a hotspot track (Koppers et al., 2021 and the references within). Figure 15 displays hotspot track models assuming a hotspot generated the Geologist Seamounts at 73 Ma (Figure 15A), 84 Ma (Figure 15B), or 90 Ma (Figure 15C) based on a fixed hotspot model from Wessel and Kroenke (2008) and a mobile hotspot model from Doubrovine et al. (2012). The mobile hotspot model considers and corrects for independent plume motion based on time dependent mantle flow models when creating their absolute plate motion model (Doubrovine et al., 2012). Based on Figure 15, the lack of observed seamount chains along the modeled hotspot track as well as the lack of correlation with the Euterpe plume (Musician Seamounts; Balbas et al., 2023) indicate that a direct mantle plume origin for any of Geologist Seamounts lava flows sampled thus far is unlikely. The only geodynamically feasible plume-seamount connection comes from the 74–73 Ma lava flows. In this hypothetical scenario the Euterpe plume would have experienced an extreme southward deflection between ~80–74 Ma in order to source the lava flows recovered from Jaggar and Cook Seamounts (Figure 15A). Extreme southward deflection of a plume has only been observed during the formation of the Emperor Seamount chain in which some authors theorized that a plume-Kula ridge release mechanism was the driver for rapid southward plume motion (e.g. Tarduno et al., 2009). As of now there is no independent evidence to support the hypothesis and as such there is no clear geochronologic/geographic correlation between Geologist Seamounts volcanism and known mantle plumes.

5.5 Shear-Driven Upwelling Origin?

Shear-driven upwelling of upper mantle material in near-ridge environments can potentially produce intraplate volcanoes arranged in age progressive chains correlated with asthenosphere velocity rather than absolute plate motion (e.g. Ballmer et al., 2013). Asthenospheric shear develops between oppositely moving asthenosphere and lithosphere; moreover, shear of low-viscosity fingers within the asthenosphere promotes upwelling of mantle material and subsequent decompression melting (Conrad et al., 2011, Ballmer et al., 2013). This process was postulated by Ballmer et al. (2013) to account for the age and geochemical characteristics across Pukapuka ridge (18°S, 113.6°W to 14°S, 141.3°W; Figure 1). Pukapuka ridge is a linear chain of seamounts and ridges that is known to lack age progressions consistent with absolute plate motion and lacks the geochemical constituents of mantle-plume derived melts (Sandwell et al., 1995; Janney et al., 2000; Ballmer et al., 2013). Pukapuka lava flows commonly display depleted trace element concentrations and high degree melting within the shallow asthenosphere (e.g. Figure 9).

The Geologist Seamounts also lack age-progressions associated with plate motion and formed above a similar region of NE SOPITA mantle near the East Pacific Rise (Figure 14); therefore, Pukapuka ridge may still be a useful modern analog to understand the origin of the Geologist Seamounts. Ballmer et al. (2013) postulates that Pukapuka ridge formed from the shear-driven upwelling of melts derived on low-viscosity fingers within the upper mantle. This proposed low-viscosity finger is moving perpendicular to the N-S orientation of the East Pacific Rise, and this would explain the E-W orientation of Pukapuka ridge (Ballmer et al., 2013). An E-W orientation would, most likely, be required for the Geologist Seamounts to originate from this process assuming paleo Pacific-Farallon spreading orientation is N-S, based on plate models from Müller et al. (2019) and Seton et al. (2020) that follow the magnetic isochron lineation's east of the Geologist Seamounts. The seamounts, instead, are oriented N-S to NE-SW; additionally, no evidence for age progressions have been observed. However, a single pulse of shear derived upwelling could be responsible for one or more of the dated eruptions. Chemically, most of the Geologist Seamount lava flows show higher degrees of LREE enrichment and elevated Dy/Yb as compared to Pukapuka ridge lavas (blue fields; Figures 9, 10). Therefore, it is unlikely that shear driven upwelling can account for chemical composition of the Geologist Seamounts as well as the ~17 m.y. of volcanism in a limited geographic region and is an unlikely driver for volcanism among the Geologist Seamounts.

5.6 Lithospheric Deformation Origin?

Lithospheric thinning by diffuse extension provides a means for decompression melting of the shallow mantle (McKenzie and Bickel, 1988; Sandwell et al., 1995). Subsequent ascent of lower lithosphere/upper asthenosphere melts may be a mechanism for intraplate seamount formation. This model is also postulated to explain the origin of Pukapuka ridge (Sandwell et al., 1995, Janney et al., 2000), as opposed to an asthenospheric shear origin (Ballmer et al., 2013). The Geologist Seamounts display the most consistent overlapping chemical characteristics with offshore California Margin seamounts that are believed to be derived from extensional processes (e.g. Castillo et al., 2010; Davis et al., 2010) (Green fields; Figures 9, 10).

To generate melting in the upper mantle a tectonic driver that generates extension perpendicular to the orientation of the seamounts is required. Sandwell et al. (1995) proposed that the stress fields generated from slab-pull were great enough to promote diffuse extension along a transform fault bounded lithospheric block that houses Pukapuka ridge near the East Pacific Rise. Extensional melting chiefly occurred in this location because it contains the youngest, and therefore, weakest lithosphere near the East Pacific Rise (Sandwell et al., 1995). Near the Geologist Seamounts, the existence of rotated abyssal hill fabrics proximal to the Geologist Seamounts (Figure 4), the Farnella Escarpment, the Kana Keoki FZ, and associated magnetic chron offsets in the Geologist Seamount region (Atwater and Severinghaus, 1989; Figure 4) indicate Pacific Plate reorganization and potential microblock formation (Sager and Pringle, 1987) was associated with initial seamount genesis during the late Cretaceous. Like Pukapuka ridge, the oldest Geologist Seamounts would have resided near the lithospheric block generated by the Molokai and Clarion/Kana Keoki transform offsets (Figure 16).

The existence of the Kana Keoki FZ indicates that there were additional stress fields that weren't completely diffused by the Molokai and Clarion transform faults during the late Cretaceous.

Additionally, rotated abyssal hill fabrics indicate a change in plate motion during the late Cretaceous potentially associated with the formation of the Kana Keoki FZ (Figure 4). The Farnella Escarpment has an enigmatic origin and may represent a pseudofault limb of a southward propagating ridge tip (e.g. Morgan and Sanwell, 1994), that may have 'jumped' at its southern limit to the Kana Keoki FZ. We propose that a Molokai and Kana Keoki transform fault bounded microblock was created due to plate reorganization and a corresponding migration of the spreading segments. A microblock, in this case, would be a segment of oceanic lithosphere that is deforming internally relative to the Pacific Plate (e.g. Li et al., 2018). The microblock's eastern bounds are not clear due to a lack of multibeam bathymetry data in the region. Nevertheless, the microblock potentially extends to the E-W extent of the Kana Keoki FZ at roughly chron C30n (68 Ma; Seton et al., 2020) based on isochron offsets first discovered by Atwater and Severinghaus (1989). The microblock's initiation (western boundary) is obscured by Hawaii although the Farnella Escarpment may be a surface expression of the microblock initiation, especially since it trends roughly perpendicular (~N, 312°) to the previously mentioned isochron offset (~N40°, Figure 4). Extension along the western ridge of a microblock may have generated volcanism voluminous enough to generate the Geologist Seamounts. Provided the Kana Keoki FZ existed from ~90–70 Ma, the age of the proposed microblock is temporally consistent with the current constraints on the age and duration of volcanism among the Geologist Seamounts (90–73 Ma).

It is unclear whether the 90–87 Ma episode of volcanism represents seamount generation on a recently extinct spreading ridge (akin to Davis Seamount at the California continental margin (Figure 1; Castillo et al., 2010) or if it is more simply near-ridge N-S rift volcanism following the pre-existing abyssal hill fabric. Figure 16 shows a schematic evolution of the Geologist Seamounts during three time slices in the late Cretaceous (employing the plate motion model from Müller et al., 2019). The Geologist Seamounts are shown as initially forming off-ridge (Figure 16A). We propose that plate reorganization at *ca.* 90 Ma (Müller et al., 2019) or 91 Ma (Wessel and Kroenke, 2008) generated a microblock that pulled on the Geologist Seamounts region lithosphere before then fusing back onto the Pacific Plate within ~20 m.y. Changes in the position of the Pacific Plate poles of rotation have been previously constrained using hotspot tracks at *ca.* 91.7, 87.1, 83.7 and 71 Ma (WK08-G; Wessel and Kroenke, 2008). It is likely that the pulses of regional extension were initiated due to the change in plate motion vectors initially around 91.7 Ma, thus generating stress that eventually initiated some local volcanism. The plate vector shift around 87 or 84 Ma then resulted local changes that further exaggerated stresses in the region and potentially led to an additional pulse of volcanism. The plate motion shift at *ca.* 71 Ma was then a final driver of volcanism in the region before a more stable local kinematic configuration developed and the Kana Keoki transform fault ended. Major changes in Pacific Plate motion associated with pulses of extensional volcanism is a rare connection; however, O'Connor et al. (2015) made a similar association with some volcanism along the Musician Seamounts elongate ridges and within the Murray fracture zone temporally corresponding to a Pacific Plate motion vector change at *ca.* 50 Ma. Nonetheless, when all available regional and chemical data is considered, the best fit model for the origin of intraplate volcanism among the Geologist Seamounts is that lithospheric deformation associated with a local microblock formation and rotation corresponding to Pacific Plate motion vector changes drove localized extension, which caused low degree melting of shallow asthenosphere ± lithosphere during the ~90-73 Ma timeframe.

6.0 Conclusions

Here we provided $^{40}Ar/^{39}Ar$ age determinations and major and trace element geochemistry of lava flows recovered from the Geologist Seamounts cluster to better understand their origin. Bathymetry maps of the cluster and nearby seafloor structures highlight morphological relationships between the seamounts and the surrounding seafloor. Age determinations in conjunction with morphology illuminate three distinct volcanic episodes: A *ca.* 90–87 Ma episode with lava flows preferentially channeled in the N-S direction, a *ca.* 84 Ma episode channeled in a NE-SW orientation, and a *ca.* 74–73 Ma episode of volcanism with no distinct channeling orientation. Lava flow ages and composition in conjunction with paleo reconstructions of seamounts allows us to propose the following conclusions regarding the origin of the Geologist Seamounts:

1. Lava flows within the Geologist Seamounts cluster are highly alkalic with all seamounts except the Northern McCall ridge displaying trace element ratios consistent with low degree, moderately deep melting of asthenosphere mantle. There is no evidence for ancient recycled crustal materials within the mantle source reservoirs that sourced Geologist Seamount volcanism.

2. There are at least 17 million years of volcanism (90–73 Ma) recorded within the Geologist Seamounts cluster whose preferential magma channeling was not consistent overtime.

3. The Geologist Seamounts overrode the fringes of the SOPITA melt zone during the first two episodes of volcanism, but was outside this zone by the time of the final episode of volcanism. Moreover, there are no known mantle plumes that correlate with the Geologist Seamounts paleo-location, nor are there any chains of seamounts that correlate with a hypothetical fixed hotspot post and pre-ceding the Geologist Seamounts that correlate to any of the three episodes of volcanism. As such, a direct mantle-plume origin is improbable for the Geologist Seamounts cluster.

4. The orientation, timing and chemical composition of volcanism within the Geologist Seamounts cluster indicate that a shear-driven upwelling origin is unlikely. Shear-driven upwelling may be able to account for one pulse of volcanism; however, this process cannot account for ~17 m.y. of volcanism in a limited geographic area.

5. The Geologist Seamounts cluster appears similar in origin to lithospheric extensional intraplate seamounts like those found on the continental margin of California. We propose that independent microblock formation and deformation drove localized extension, which caused volcanism responsible for the genesis of the Geologist Seamounts. Further work is required to calibrate local stress fields associated with plate vector shifts; however, the extension potentially occurred in pulses associated with major changes in Pacific Plate motion during the late Cretaceous.

Acknowledgements

This work represents the cumulated MS thesis research of B.S. The samples used in this study were generously provided by the Oregon State University Marine Geology Repository and Jasper Konter through the University of Hawaii. We thank the captain and crew of the R/V *Okeanos Explorer* during expedition EX1504L3. We are grateful for helpful discussions with Rob Pockalny. Kathy Zanetti is thanked for assistance with the age determination experiments. Tyrone Rooney and Todd Lydic are thanked for the whole rock geochemical analyses. We are indebted to Arya Udry and Andrew Martin for providing valuable comments and suggestions on an earlier version of this work. This work was supported by NSF-OCE Award #2121834.

Open Research

Analytical data for new samples used in this study are archived in the SESAR and EarthChem databases and will be made available prior to publication. All data used in this study is presented in Tables 3 and 4 and the Supplemental Document. Major element data for Cook Seamount lava flows from Friesen (1987). Some age determinations are from Sager and Pringle (1987).

References

Atwater, T., Sclater, J., Sandwell, D., Severinghaus, J., and Marlow, M.S., 1993, Fracture Zone Traces Across the North Pacific Cretaceous Quiet Zone and their Tectonic Implications, *in* The Mesozoic Pacific: Geology, Tectonics, and Volcanism, American Geophysical Union (AGU), p. 137–154, doi:10.1029/GM077p0137.

Atwater, T., 1989, Plate tectonic history of the northeast Pacific and western North America, *in* Winterer, E.L., Hussong, D.M., and Decker, R.W. eds., The Eastern Pacific Ocean and Hawaii, Geological Society of America, v. N, p. 0, doi:10.1130/DNAG-GNA-N.21.

Atwater, T., and Severinghaus, J., 1989, Tectonic maps of the northeast Pacific, *in* Winterer, E.L., Hussong, D.M., and Decker, R.W. eds., The Eastern Pacific Ocean and Hawaii, Geological Society of America, v. N, p. 0, doi:10.1130/DNAG-GNA-N.15.

Balbas, A., Jung, C., and Konrad, K., 2023, The origin of the Musicians Seamount Province and its inferences for Late Cretaceous Pacific Plate Motion: Marine Geology, v. 465, p. 107166, doi:10.1016/j.margeo.2023.107166.

Ballmer, M.D., Conrad, C.P., Smith, E.I., and Harmon, N., 2013, Non-hotspot volcano chains produced by migration of shear-driven upwelling toward the East Pacific Rise: Geology, v. 41, p. 479–482, doi:10.1130/G33804.1.

Barckhausen, U., Bagge, M., and Wilson, D.S., 2013, Seafloor spreading anomalies and crustal ages of the Clarion-Clipperton Zone: Marine Geophysical Research, v. 34, p. 79–88, doi:10.1007/s11001-013-9184-6.

Bienvenu, P., Bougault, H., Joron, J.L., Treuil, M., and Dmitriev, L., 1990, MORB alteration: Rare-earth element/non-rare-earth hygromagmaphile element fractionation: Chemical Geology, v. 82, p. 1–14, doi:10.1016/0009-2541(90)90070-N.

Burke, K., Steinberger, B., Torsvik, T.H., and Smethurst, M.A., 2008, Plume Generation Zones at the margins of Large Low Shear Velocity Provinces on the core–mantle boundary: Earth and Planetary Science Letters, v. 265, p. 49–60, doi:10.1016/j.epsl.2007.09.042.

Castillo, P.R., Clague, D.A., Davis, A.S., and Lonsdale, P.F., 2010, Petrogenesis of Davidson Seamount lavas and its implications for fossil spreading center and intraplate magmatism in the eastern Pacific: DAVIDSON FOSSIL SPREADING CENTER LAVA PETROGENESIS: Geochemistry, Geophysics, Geosystems, v. 11, p. n/a-n/a, doi:10.1029/2009GC002992.

Conrad, C.P., Bianco, T.A., Smith, E.I., and Wessel, P., 2011, Patterns of intraplate volcanism controlled by asthenospheric shear: Nature Geoscience, v. 4, p. 317–321, doi:10.1038/ngeo1111.

Constable, S., and Heinson, G., 2004, Hawaiian hot-spot swell structure from seafloor MT sounding: Tectonophysics, v. 389, p. 111–124, doi:10.1016/j.tecto.2004.07.060.

Chaytor, J.D., Keller, R.A., Duncan, R.A., and Dziak, R.P., 2007, Seamount morphology in the Bowie and Cobb hot spot trails, Gulf of Alaska: HOT SPOT TRAIL SEAMOUNT MORPHOLOGY: Geochemistry, Geophysics, Geosystems, v. 8, p. n/a-n/a, doi:10.1029/2007GC001712.

Darwin, C., 1842, The Structure and Distribution of Coral Reefs, John Murray, London, doi:10.1525/9780520327337.

Davis, A.S., Clague, D.A., Paduan, J.B., Cousens, B.L., and Huard, J., 2010, Origin of volcanic seamounts at the continental margin of California related to changes in plate margins: ORIGIN OF SEAMOUNTS OFFSHORE CALIFORNIA: Geochemistry, Geophysics, Geosystems, v. 11, p. n/a-n/a, doi:10.1029/2010GC003064.

Doubrovine, P.V., Steinberger, B., and Torsvik, T.H., 2012, Absolute plate motions in a reference frame defined by moving hot spots in the Pacific, Atlantic, and Indian oceans: Journal of Geophysical Research: Solid Earth, v. 117, doi:10.1029/2011JB009072.

Dymond, J., and L. Windom, H., 1968, Cretaceous K-Ar ages from Pacific Ocean seamounts: Earth and Planetary Science Letters, v. 4, p. 47–52, doi:10.1016/0012-821X(68)90052-6.

French, S.W., and Romanowicz, B., 2015, Broad plumes rooted at the base of the Earth's mantle beneath major hotspots: Nature, v. 525, p. 95–99, doi:10.1038/nature14876.

Friesen, W., 1987, Preliminary petrology of igneous and sedimentary rocks recovered from central Pacific seamounts: US Department of the Interior, US Geological Survey.

Gale, A., Dalton, C.A., Langmuir, C.H., Su, Y., and Schilling, J.-G., 2013, The mean composition of ocean ridge basalts: Geochemistry, Geophysics, Geosystems, v. 14, p. 489–518, doi:10.1029/2012GC004334.

Geldmacher, J., Hauff, F., Dürkefälden, A., Sano, T., Garbe-Schönberg, D., Portnyagin, M., and Hoernle, K., 2023, The effects of submarine alteration and phosphatization on igneous rocks: Implications for Sr-, Nd-, Pb-isotope studies: Chemical Geology, v. 631, p. 121509, doi:10.1016/j.chemgeo.2023.121509.

Gevorgian, J., Sandwell, D.T., Yu, Y., Kim, S.-S., and Wessel, P., 2023, Global Distribution and Morphology of Small Seamounts: Earth and Space Science, v. 10, p. e2022EA002331, doi:10.1029/2022EA002331.

Gradstein, F.M., Agterberg, F.P., Ogg, J.G., Hardenbol, J., van Veen, P., Thierry, J., and Huang, Z., 1994, A Mesozoic time scale: Journal of Geophysical Research: Solid Earth, v. 99, p. 24051–24074, doi:10.1029/94JB01889.

Granot, R., Cande, S.C., and Gee, J.S., 2009, The implications of long-lived asymmetry of remanent magnetization across the North Pacific fracture zones: Earth and Planetary Science Letters, v. 288, p. 551–563, doi:10.1016/j.epsl.2009.10.017.

Haase, K.M., Beier, C., and Kemner, F., 2019, A Comparison of the Magmatic Evolution of Pacific Intraplate Volcanoes: Constraints on Melting in Mantle Plumes: Frontiers in Earth Science, v. 6, p. 242, doi:10.3389/feart.2018.00242.

Handschumacher, D.W., and Andrews, J.E., 1975, Kana Keoki Fracture Zone: Interaction with the Hawaiian Ridge: Geology, v. 3, p. 25–28, doi:10.1130/0091-7613(1975)3<25:KKFZIW>2.0.CO;2.

Hess, H.H., 1946, Drowned ancient islands of the Pacific Basin: American Journal of Science, v. 244, p. 772–791, doi:10.2475/ajs.244.11.772.

Hillier, J.K., and Watts, A.B., 2007, Global distribution of seamounts from ship-track bathymetry data: Geophysical Research Letters, v. 34, doi:10.1029/2007GL029874.

Hosseini, K., Matthews, K.J., Sigloch, K., Shephard, G.E., Domeier, M., and Tsekhmistrenko, M., 2018, SubMachine: Web-Based Tools for Exploring Seismic Tomography and Other Models of Earth's Deep Interior: Geochemistry, Geophysics, Geosystems, v. 19, p. 1464–1483, doi:10.1029/2018GC007431.

Hofmann, A.W., 2003, Sampling Mantle Heterogeneity through Oceanic Basalts: Isotopes and Trace Elements: Treatise on Geochemistry, v. 2, p. 568, doi:10.1016/B0-08-043751-6/02123-X.

Holcomb, R.T., and Robinson, J.E., 2004, Maps of Hawaiian Islands Exclusive Economic Zone interpreted from GLORIA sidescan-sonar imagery: US Department of the Interior, US Geological Survey.

Janney, P.E., Macdougall, J.D., Natland, J.H., and Lynch, M.A., 2000, Geochemical evidence from the Pukapuka volcanic ridge system for a shallow enriched mantle domain beneath the South Pacific Superswell: Earth and Planetary Science Letters, v. 181, p. 47–60, doi:10.1016/S0012-821X(00)00181-3.

Johansson, L., Zahirovic, S., and Müller, R.D., 2018, The Interplay Between the Eruption and Weathering of Large Igneous Provinces and the Deep-Time Carbon Cycle: Geophysical Research Letters, v. 45, p. 5380–5389, doi:10.1029/2017GL076691.

Konrad, K., Koppers, A.A.P., Steinberger, B., Finlayson, V.A., Konter, J.G., and Jackson, M.G., 2018, On the relative motions of long-lived Pacific mantle plumes: Nature Communications, v. 9, p. 854, doi:10.1038/s41467-018-03277-x.

Konrad, K. SESAR Data Archive, to be released post manuscript acceptance. SESAR

Konter, J.G., Hanan, B.B., Blichert-Toft, J., Koppers, A.A.P., Plank, T., and Staudigel, H., 2008, One hundred million years of mantle geochemical history suggest the retiring of mantle plumes is premature: Earth and Planetary Science Letters, v. 275, p. 285–295, doi:10.1016/j.epsl.2008.08.023.

Koppers, A.A.P., Becker, T.W., Jackson, M.G., Konrad, K., Müller, R.D., Romanowicz, B., Steinberger, B., and Whittaker, J.M., 2021, Mantle plumes and their role in Earth processes: Nature Reviews Earth & Environment, v. 2, p. 382–401, doi:10.1038/s43017-021-00168-6.

Koppers, A., and Watts, A., 2010, Intraplate Seamounts as a Window into Deep Earth Processes: Oceanography, v. 23, p. 42–57, doi:10.5670/oceanog.2010.61.

Koppers, A.A.P., 2002, ArArCALC—software for 40Ar/39Ar age calculations: Computers & Geosciences, v. 28, p. 605–619, doi:10.1016/S0098-3004(01)00095-4.

Kuiper, K.F., Deino, A., Hilgen, F.J., Krijgsman, W., Renne, P.R., and Wijbrans, J.R., 2008, Synchronizing Rock Clocks of Earth History: Science, v. 320, p. 500–504, doi:10.1126/science.1154339.

Le Bas, M.J., Le Maitre, R.W., Streckeisen, A., Zanettin, B., and IUGS Subcommission on the Systematics of Igneous Rocks, 1986, A Chemical Classification of Volcanic Rocks Based on the Total Alkali-Silica Diagram: Journal of Petrology, v. 27, p. 745–750, doi:10.1093/petrology/27.3.745.

Li, S. et al., 2018, Microplate tectonics: new insights from micro-blocks in the global oceans, continental margins and deep mantle: Earth-Science Reviews, v. 185, p. 1029–1064, doi:10.1016/j.earscirev.2018.09.005.

Ludden, J.N., and Thompson, G., 1979, An evaluation of the behavior of the rare earth elements during the weathering of sea-floor basalt: Earth and Planetary Science Letters, v. 43, p. 85–92, doi:10.1016/0012-821X(79)90157-2.

Mammerickx, J., Naar, D.F., and Tyce, R.L., 1988, The mathematician paleoplate: Journal of Geophysical Research: Solid Earth, v. 93, p. 3025–3040, doi:10.1029/JB093iB04p03025.

Mather, B., Müller, D., Seton, M., Ruttor, S., Nebel, O., and Mortimer, N., 2020, Intraplate volcanism triggered by bursts in slab flux: SCIENCE ADVANCES, v. 6, p. 9, doi:10.1126/sciadv.abd0953.

Matthews, K.J., Dietmar Müller, R., and Sandwell, D.T., 2016, Oceanic microplate formation records the onset of India–Eurasia collision: Earth and Planetary Science Letters, v. 433, p. 204–214, doi:10.1016/j.epsl.2015.10.040.

Mayer, L., Jakobsson, M., Allen, G., Dorschel, B., Falconer, R., Ferrini, V., Lamarche, G., Snaith, H., and Weatherall, P., 2018, The Nippon Foundation—GEBCO Seabed 2030 Project: The Quest to See the World’s Oceans Completely Mapped by 2030: Geosciences, v. 8, p. 63, doi:10.3390/geosciences8020063.

McDonough, W.F., and Sun, S. -s., 1995, The composition of the Earth: Chemical Geology, v. 120, p. 223–253, doi:10.1016/0009-2541(94)00140-4.

Mckenzie, D., and O’nions, R.K., 1991, Partial Melt Distributions from Inversion of Rare Earth Element Concentrations: Journal of Petrology, v. 32, p. 1021–1091, doi:10.1093/petrology/32.5.1021.

Mckenzie, D., and Bickle, M.J., 1988, The Volume and Composition of Melt Generated by Extension of the Lithosphere: Journal of Petrology, v. 29, p. 625–679, doi:10.1093/petrology/29.3.625.

Min, K., Mundil, R., Renne, P.R., and Ludwig, K.R., 2000, A test for systematic errors in 40Ar/39Ar geochronology through comparison with U/Pb analysis of a 1.1-Ga rhyolite: Geochimica et Cosmochimica Acta, v. 64, p. 73–98, doi:10.1016/S0016-7037(99)00204-5.

Mitchell, N.C., 2001, Transition from circular to stellate forms of submarine volcanoes: Journal of Geophysical Research: Solid Earth, v. 106, p. 1987–2003, doi:10.1029/2000JB900263.

Morgan, W.J., 1971, Convection Plumes in the Lower Mantle: Nature, v. 230, p. 42–43, doi:10.1038/230042a0.

Morgan, J.P. and Sandwell, D.T., 1994. Systematics of ridge propagation south of 30 S. Earth and Planetary Science Letters, v. 121(1-2), p.245-258, doi: 10.1016/0012-821X(94)90043-4

Müller, R.D. et al., 2019, A Global Plate Model Including Lithospheric Deformation Along Major Rifts and Orogens Since the Triassic: Tectonics, v. 38, p. 1884–1907, doi:10.1029/2018TC005462.

O’Connor, J.M., Hoernle, K., Müller, R.D., Morgan, J.P., Butterworth, N.P., Hauff, F., Sandwell, D.T., Jokat, W., Wijbrans, J.R., and Stoffers, P., 2015, Deformation-related volcanism in the Pacific Ocean linked to the Hawaiian–Emperor bend: Nature Geoscience, v. 8, p. 393–397, doi:10.1038/ngeo2416.

Pringle, M.S.J., 1992, Geochronology and petrology of the Musicians Seamounts, and the search for hot spot volcanism in the Cretaceous Pacific [Ph.D. thesis]: University of Hawaii at Manoa, 235 p.

Rooney, T.O., Franceschi, P., and Hall, C.M., 2011, Water-saturated magmas in the Panama Canal region: a precursor to adakite-like magma generation? Contributions to Mineralogy and Petrology, v. 161, p. 373–388, doi:10.1007/s00410-010-0537-8.

Rooney, T.O., Morell, K.D., Hidalgo, P., and Fraceschi, P., 2015, Magmatic consequences of the transition from orthogonal to oblique subduction in Panama: Geochemistry, Geophysics, Geosystems, v. 16, p. 4178–4208, doi:10.1002/2015GC006150.

Sager, W.W., and Pringle, M.S., 1987, Paleomagnetic constraints on the origin and evolution of the Musicians and South Hawaiian seamounts, central Pacific Ocean: Seamounts, Islands, and Atolls, v. 43, p. 133–162, doi:10.1029/GM043p0133.

Sandwell, D.T., Winterer, E.L., Mammerickx, J., Duncan, R.A., Lynch, M.A., Levitt, D.A., and Johnson, C.L., 1995, Evidence for diffuse extension of the Pacific Plate from Pukapuka ridges and cross-grain gravity lineations: Journal of Geophysical Research: Solid Earth, v. 100, p. 15087–15099, doi:10.1029/95JB00156.

Seton, M., Müller, R.D., Zahirovic, S., Williams, S., Wright, N.M., Cannon, J., Whittaker, J.M., Matthews, K.J., and McGirr, R., 2020, A Global Data Set of Present-Day Oceanic Crustal Age and Seafloor Spreading Parameters: Geochemistry, Geophysics, Geosystems, v. 21, p. e2020GC009214, doi:10.1029/2020GC009214.

Smoot, N.C., 1995, Mass wasting and subaerial weathering in guyot formation: the Hawaiian and Canary Ridges as examples: Geomorphology, v. 14, p. 29–41, doi:10.1016/0169-555X(95)00035-4.

Staudigel, H., Park, K.-H., Pringle, M., Rubenstone, J.L., Smith, W.H.F., and Zindler, A., 1991, The longevity of the South Pacific isotopic and thermal anomaly: Earth and Planetary Science Letters, v. 102, p. 24–44, doi:10.1016/0012-821X(91)90015-A.

Stracke, A., Willig, M., Genske, F., Béguelin, P., and Todd, E., 2022, Chemical Geodynamics Insights From a Machine Learning Approach: Geochemistry, Geophysics, Geosystems, v. 23, p. e2022GC010606, doi:10.1029/2022GC010606.

Tarduno, J., Bunge, H.-P., Sleep, N., and Hansen, U., 2009, The Bent Hawaiian-Emperor Hotspot Track: Inheriting the Mantle Wind: Science, v. 324, p. 50–53, doi:10.1126/science.1161256.

Tebbens, S.F., Cande, S.C., Kovacs, L., Parra, J.C., LaBrecque, J.L., and Vergara, H., 1997, The Chile ridge: A tectonic framework: Journal of Geophysical Research: Solid Earth, v. 102, p. 12035–12059, doi:10.1029/96JB02581.

Wessel, P., and Kroenke, L.W., 2008, Pacific absolute plate motion since 145 Ma: An assessment of the fixed hot spot hypothesis: Journal of Geophysical Research, v. 113, p. B06101, doi:10.1029/2007JB005499.

Wessel, P., and Kroenke, L., 1997, A geometric technique for relocating hotspots and refining absolute plate motions: Nature, v. 387, p. 365–369, doi:10.1038/387365a0.

Willbold, M., and Stracke, A., 2006, Trace element composition of mantle end-members: Implications for recycling of oceanic and upper and lower continental crust: Geochemistry, Geophysics, Geosystems, v. 7, p. 2005GC001005, doi:10.1029/2005GC001005.

Wright, J., and Rothery, D.A., 1998, Chapter 4 - The structure and formation of oceanic lithosphere, *in* Wright, J. and Rothery, D.A. eds., The Ocean Basins: Their Structure and Evolution (Second Edition), Oxford, Butterworth-Heinemann, Open University Oceanography, p. 68–95, doi:https://doi.org/10.1016/B978-075063983-5/50005-9

Zindler, A., and Hart, S., 1986, Chemical Geodynamics: Annual Review of Earth and Planetary Sciences, v. 14, p. 493, doi:10.1146/annurev.ea.14.050186.002425.

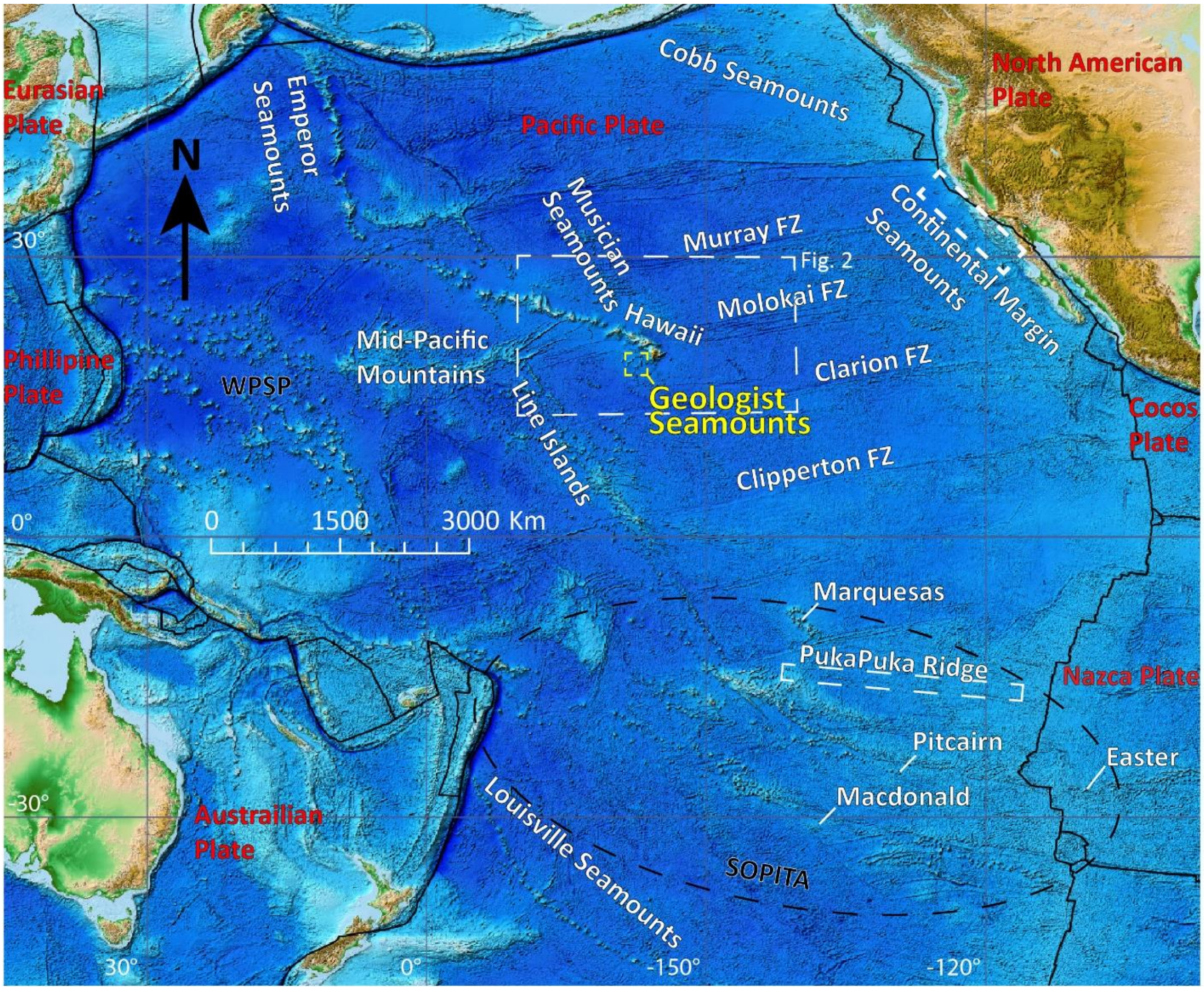

Figure 1: Bathymetric map of the Pacific Basin with key features labeled. The extent of figure 2 is noted. FZ = Fracture Zone. SOPITA = Southern Pacific Isotopic and Thermal Anomaly. WPSP = Western Pacific Seamount Province. Solid black lines are plate boundaries.

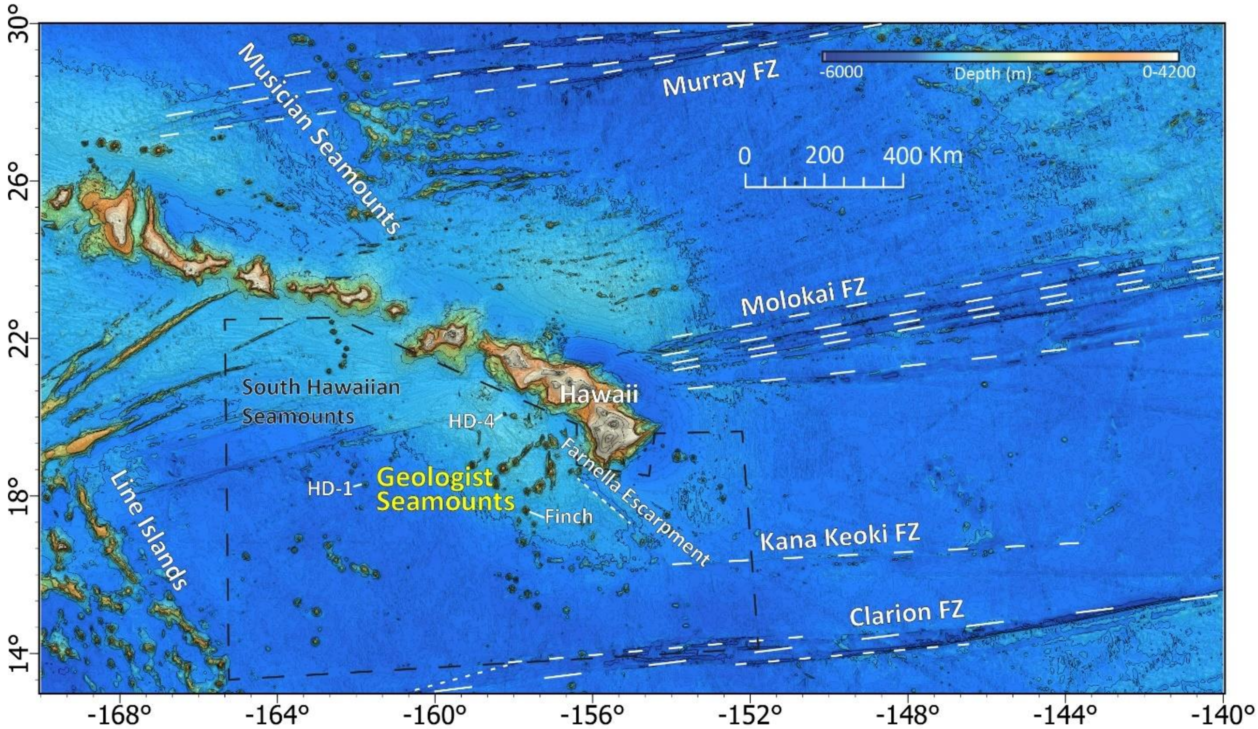

Figure 2: Regional bathymetric map of the South Hawaiian Seamount Province and nearby labeled key features. White dashed lines are linear seafloor features. Black dashed lines are the extent of the South Hawaiian Seamounts defined in this study. FZ = Fracture Zone.

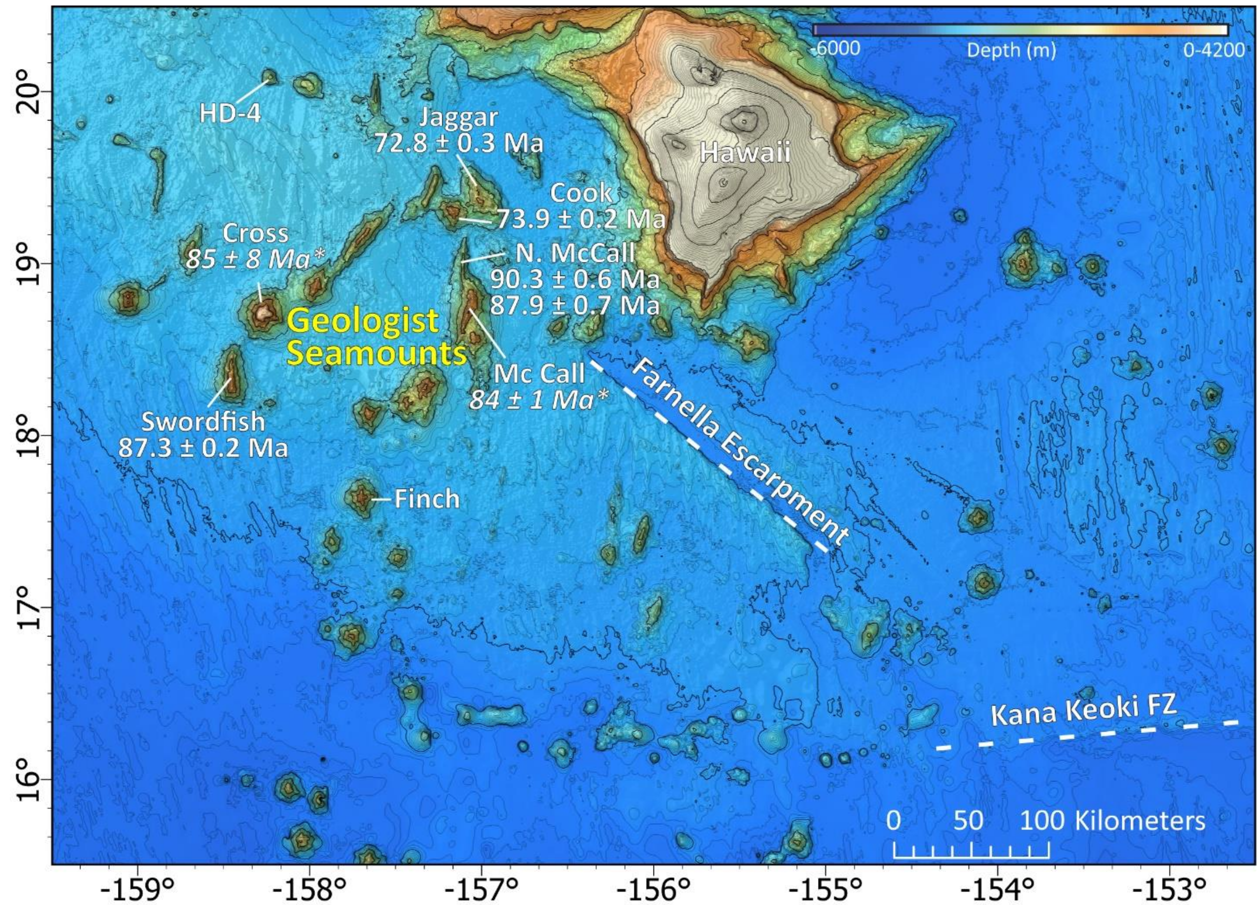

Figure 3: Bathymetry map of the Geologist Seamounts, Farnella Escarpment, and the Kana Keoki fracture zone. White dashed lines are linear seafloor features. FZ = Fracture Zone. Age determinations from this study, except for Cross and Central McCall, which are best estimates from Sager and Pringle (1987). See Supplemental Document One for more detailed individual seamount morphologies and recovered sample information.

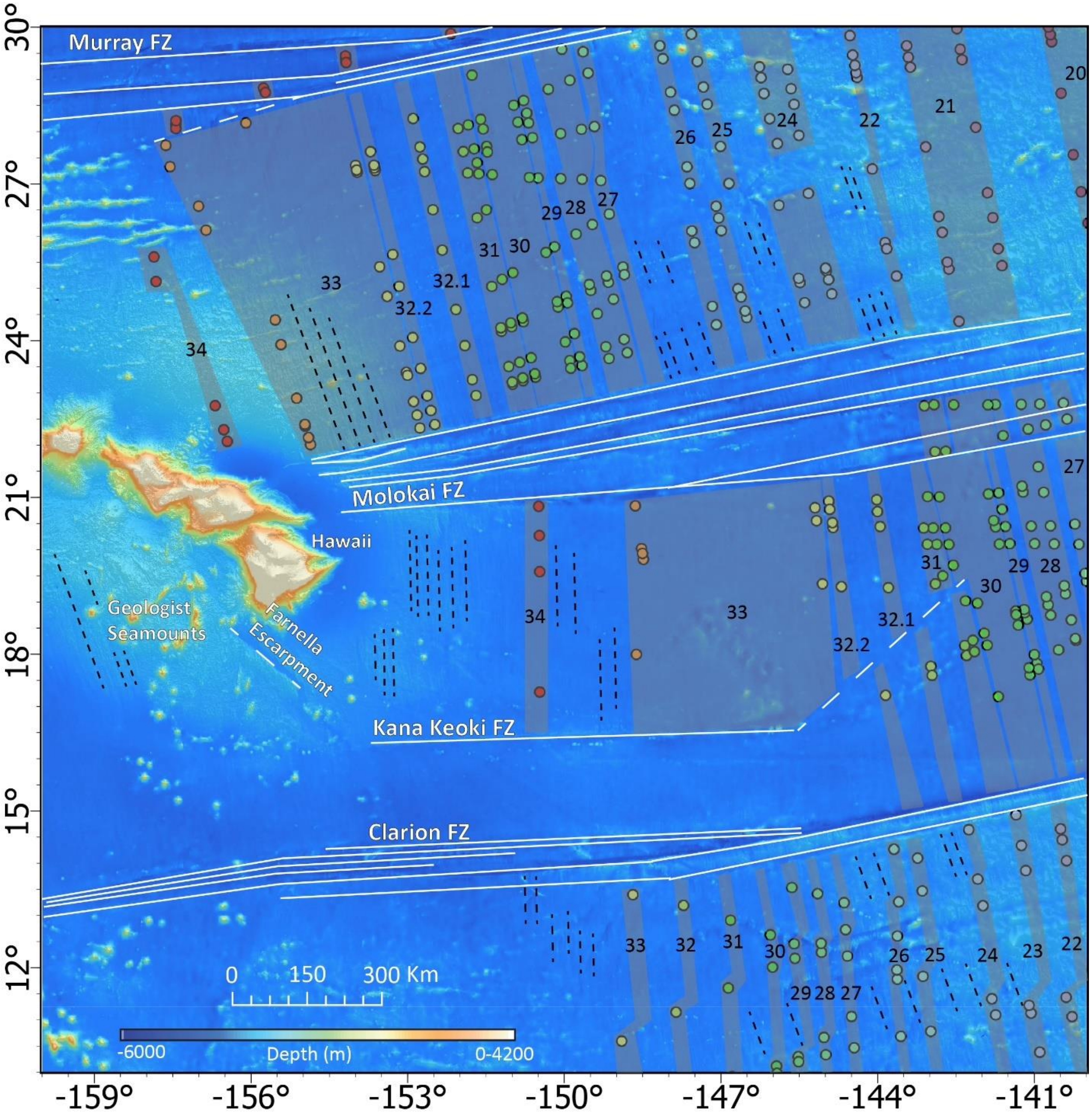

Figure 4: A map of magnetic picks and abyssal hill fabrics near Hawaii and the Geologist Seamounts adapted from Atwater (1989). Colored circles are magnetic picks colored based on assigned chron (e.g. 34, red). Magnetic pick data from Atwater and Severinghaus (1989), Barckhausen et al. (2013), and Granot et al. (2009), and ages can be found in Seton et al. (2020). Grey boxes are perceived seafloor extent of chrons based on magnetic pick information, and black numbers indicate chron number. White solid lines are fracture zones, white dashed lines are observed offsets between chrons, and black dashed lines are observed abyssal hill fabric traces. Chron 34 represents the beginning of the Paleomagnetic Quiet Zone Superchron (121-84 Ma; Gradstein et al., 1994), a period of no magnetic reversals, which usually aid in identifying seafloor ages. There is a significant offset between chrons 32.2, 32.1, 31, and 30 east of the Kana Keoki fracture zone first identified by Atwater and Severinghaus (1989).

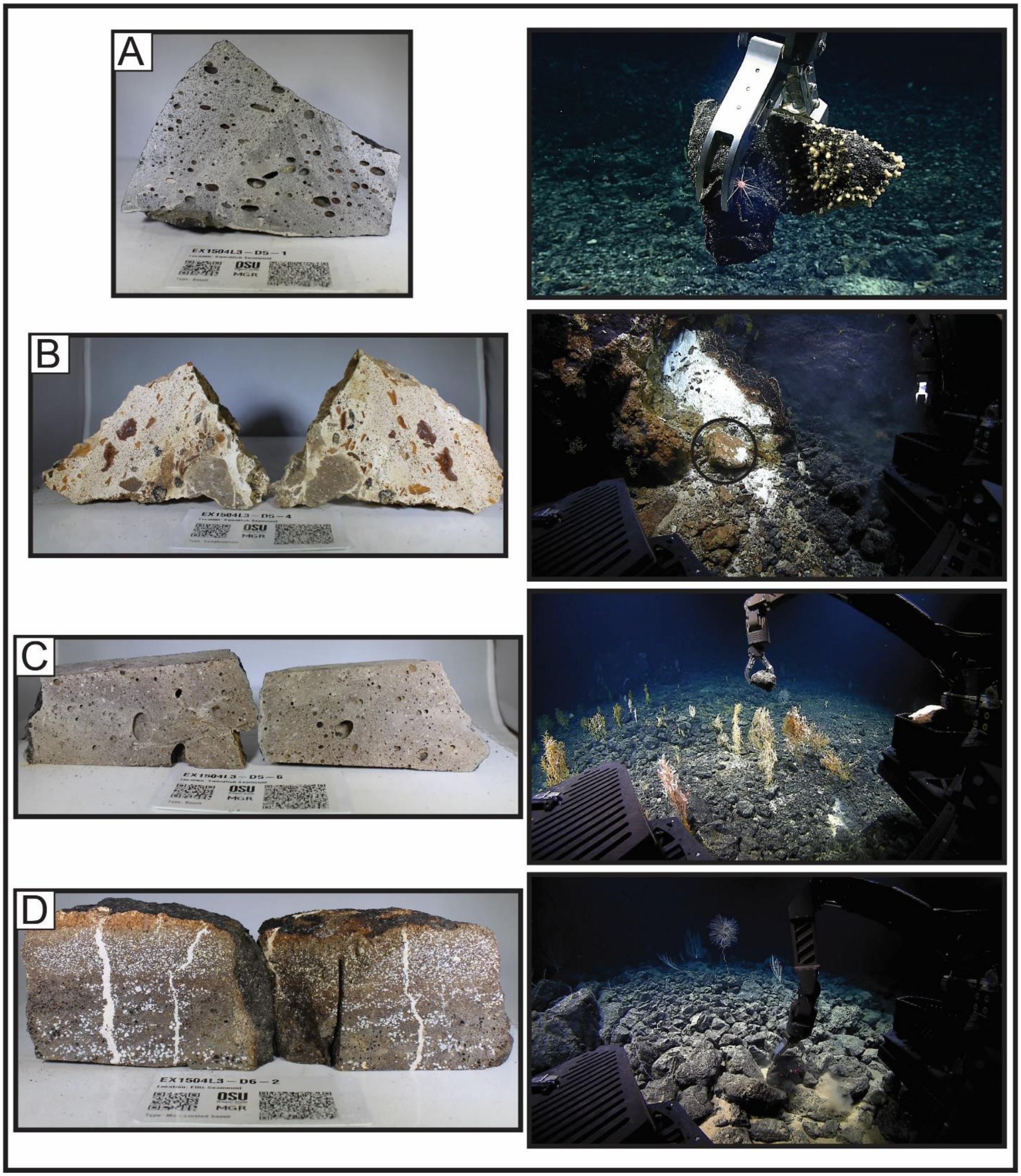
A
EX1504L3 — D5 — 1
OSU
MGR
B
EX1504L3 — D5 — 4
OSU
MGR
C
EX1504L3 — D5 — 6
OSU
MGR
D
EX1504L3 — D6 — 2
Location: Ellis Seamount
OSU
MGR

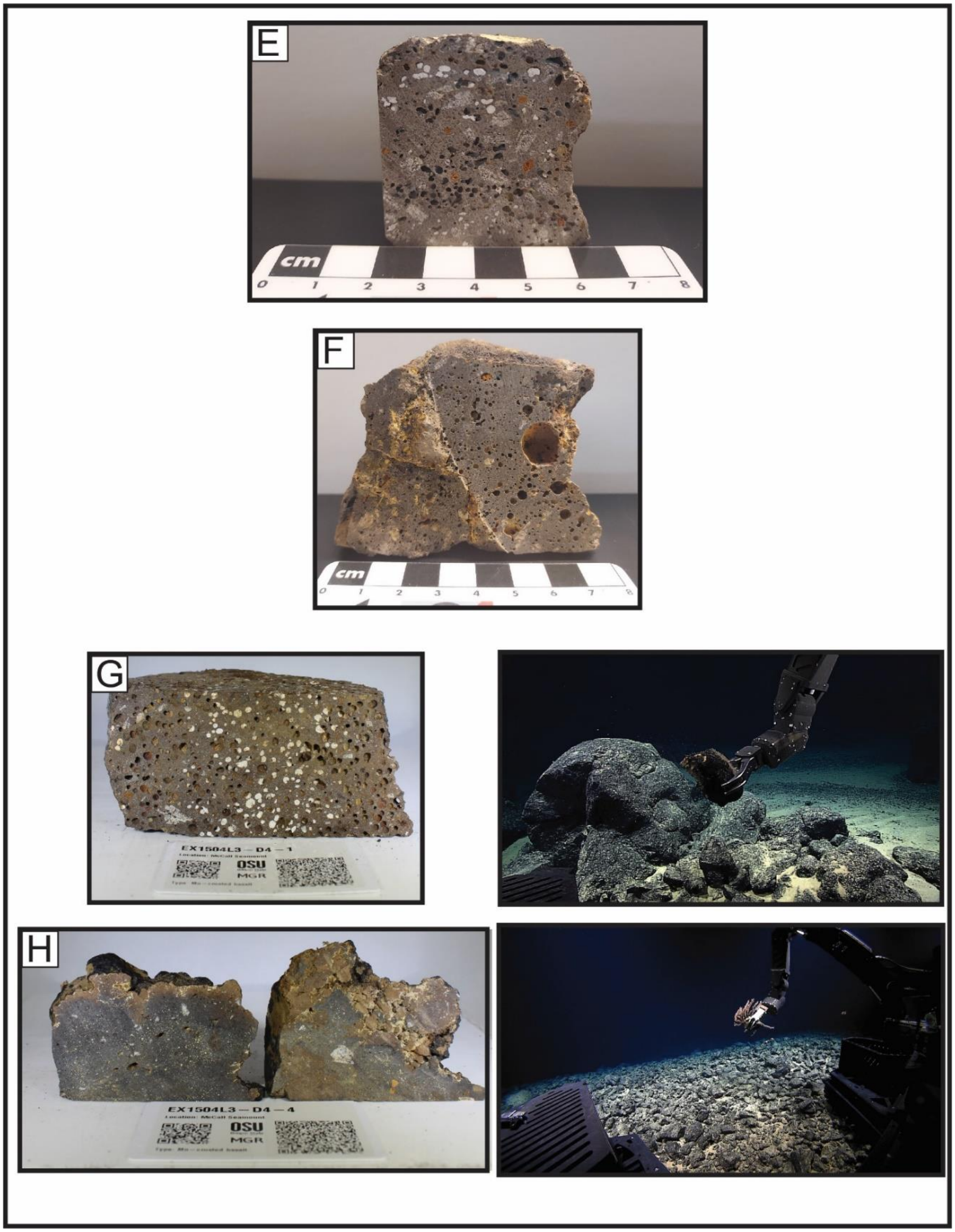

Figure 5: Hand sample (left) and ROV-grabbed (right) images of eight samples. (A) EX1504L3-D5-1. (B) EX1504L3-D5-4. Black circle (right) is the sample in-situ. (C) EX1504L3-D5-6. (D) EX1504L3-D6-2. (E) KK840824-02 STA76 RD45. This sample was dredged so there is no in-situ image. (F) KK840824-02 STA77 RD46. This sample was dredged so there is no in-situ image. (G) EX1504L3-D4-1. (H) EX1504L3-D4-4. EX1504 whole rock photos courtesy of the Oregon State University Marine Geology Repository and *in-situ* sampling images courtesy of NOAA-OR.

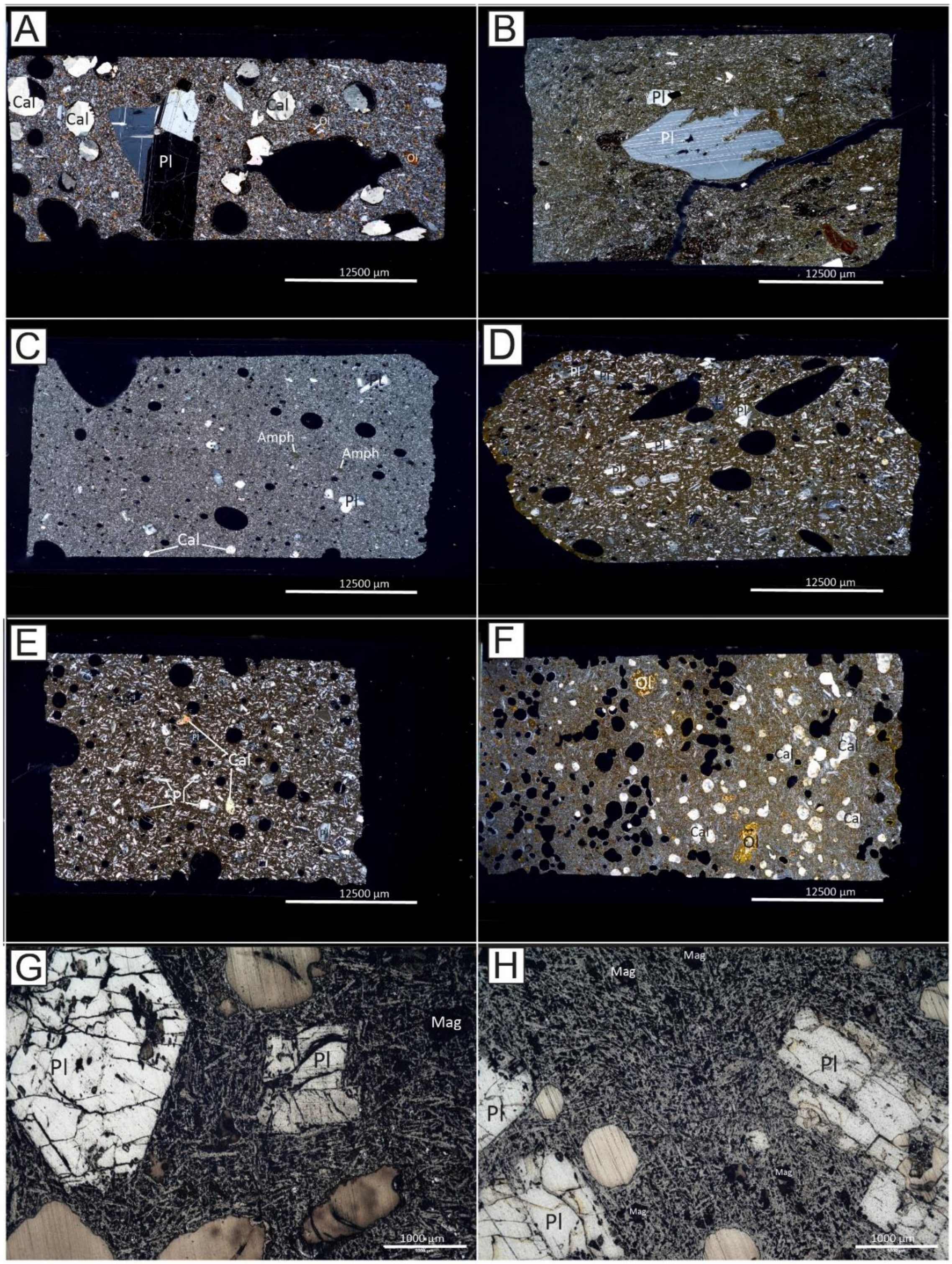

Figure 5: Representative cross-polarized thin sections of lava flows analyzed in this study. (A) EX1504L3-D4-1. (B) EX1504L3-D4-4. (C) EX1504L3-D5-1. (D) EX1504L3-D5-4. (E) EX1504L3-D5-6. (F) EX1504L3-D6-2. (G) KK840824-02 STA76 RD45. (H) KK840824-02 STA77 RD46. Pl = Plagioclase, Cal = Calcite, Ol = Olivine, Amph = Amphibole, Mag = Magnetite. Thin sections A–F originally pictured and described by OSU-MGR with updated descriptions provided herein.

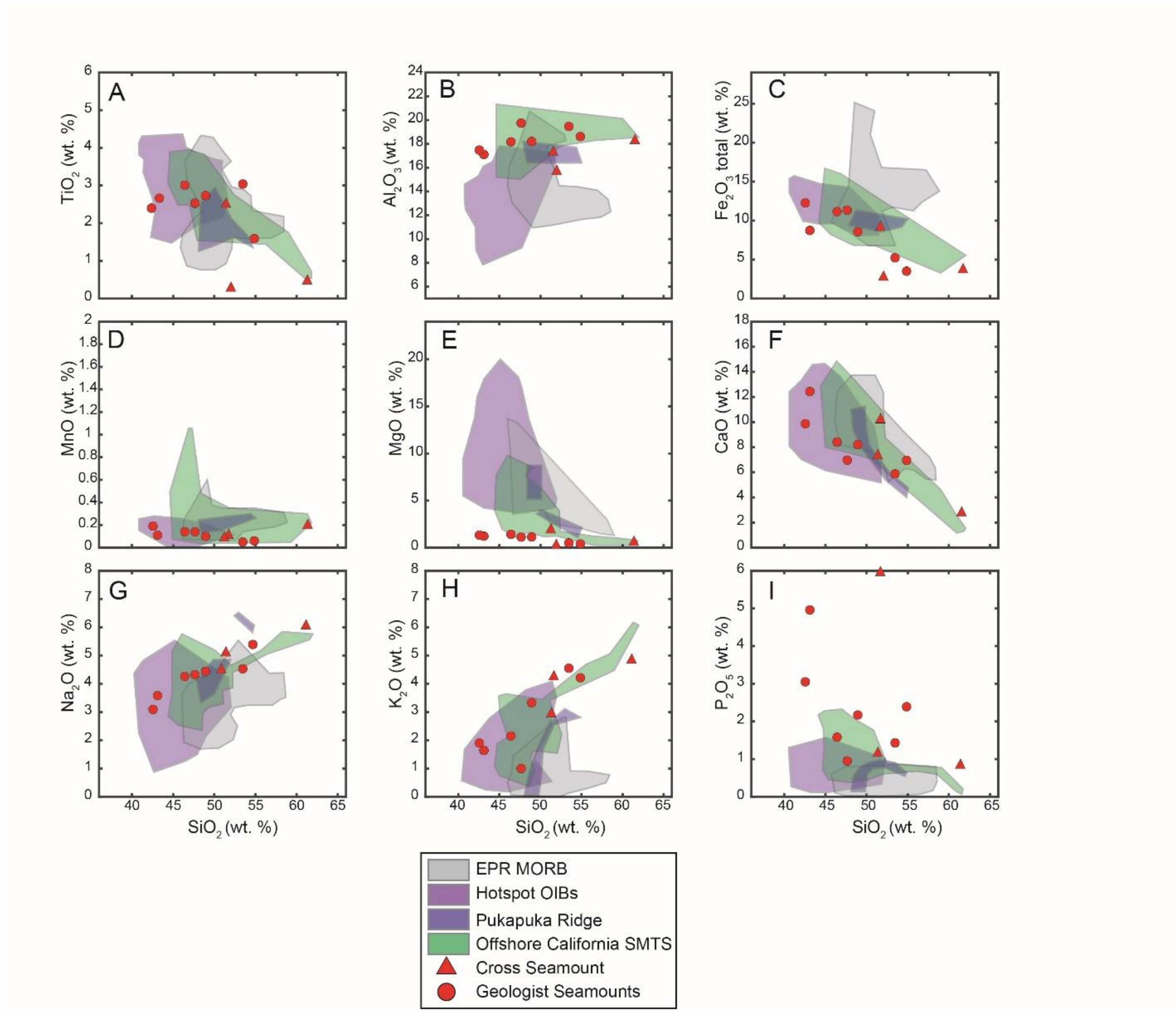

Figure 7: Major element bivariate diagrams. Red circles are from this study, and red triangles are lava flows from Cross Seamount from Friesen (1987). The envelopes for East Pacific Rise (EPR) mid-ocean ridge basalt (MORB) (Stracke et al., 2022), hotspot derived ocean island basalts (OIBs) (Willbold and Stracke, 2006), Pukapuka Ridge (Janney et al., 2000) and Offshore California Seamounts (Davis et al., 2010) are shown.

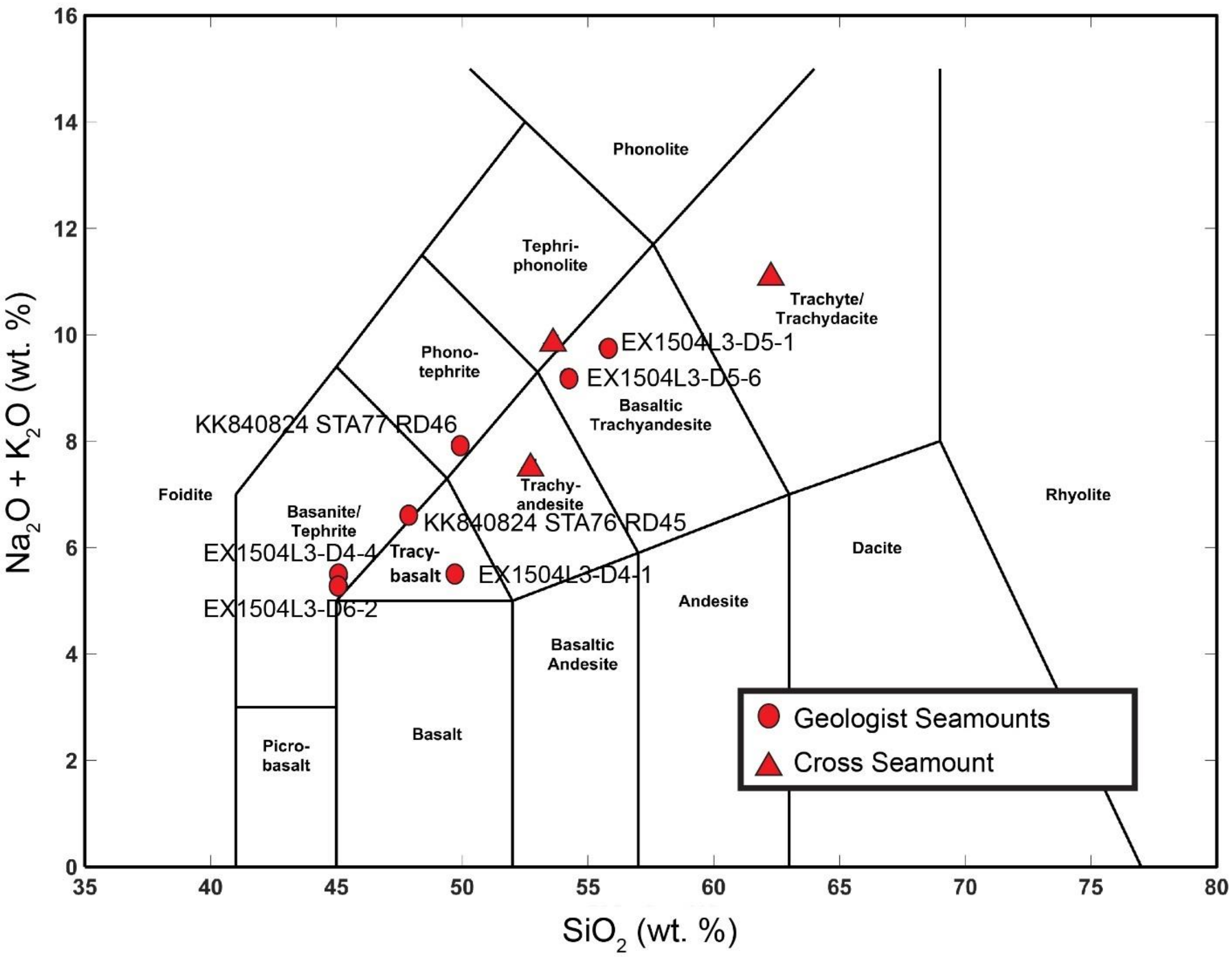

Figure 8: Total alkali silica diagram (classification scheme from Le Bas, 1986). Red circles are from this study, and red triangles are lava flows from Cross Seamount from Friesen (1987).

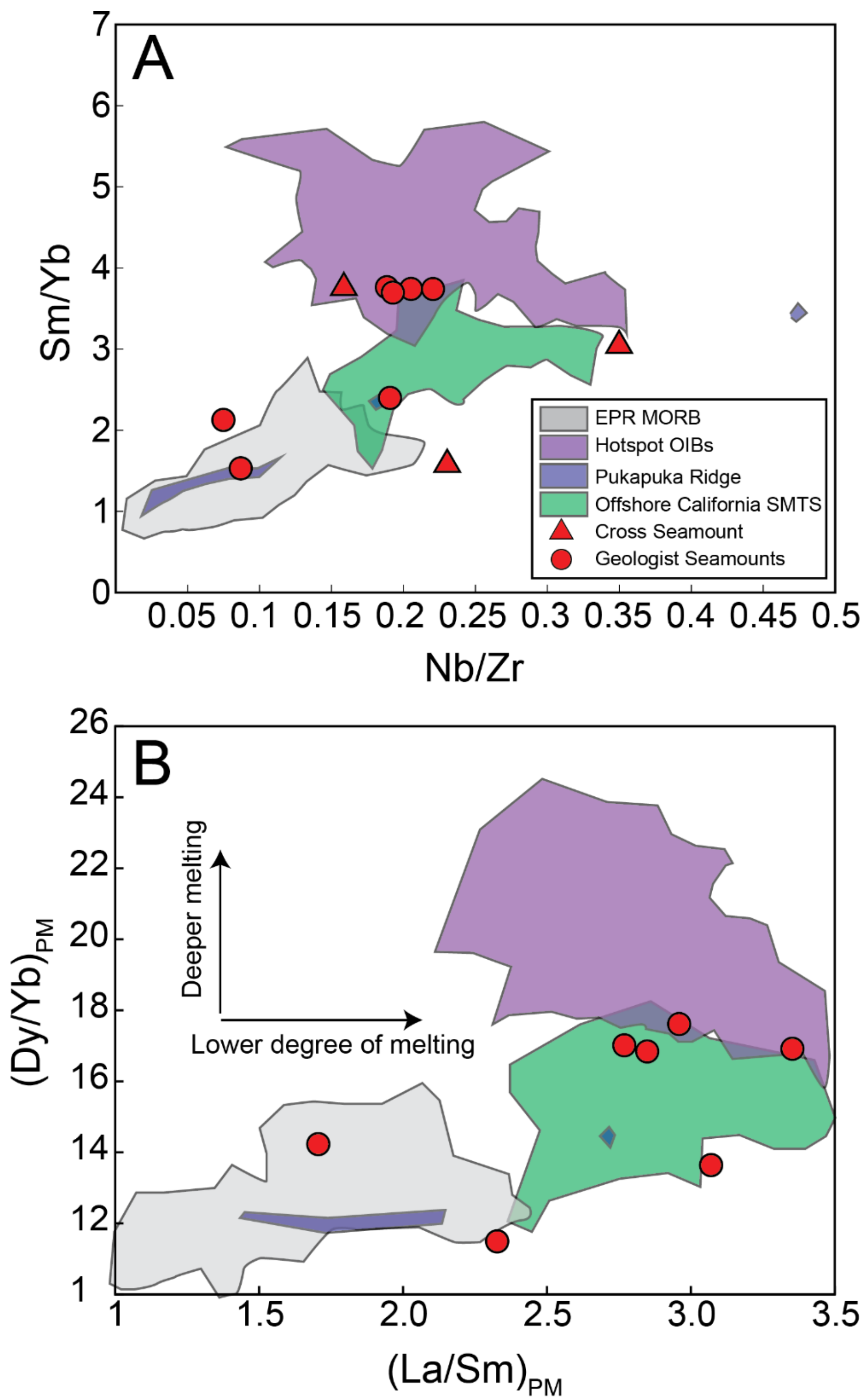

Figure 9: Key trace element ratios for the Geologist Seamount lavas compared to relevant compositional fields. **(**A) Sm/Yb vs. Nb/Zr diagram. Red triangles are from Friesen (1987) and do not contain a full suite of trace element concentration. (B) $(Dy/Yb)_{PM}$ vs. $(La/Sm)_{PM}$ diagram. PM = Primitive Mantle. PM values are from McDonough and Sun (1995). Trends for depth of melting and degree of melting are shown. The first order controls and trends for HREE and LREE ratios are shown in (B). Symbols and envelopes are the same as in Figure 7.

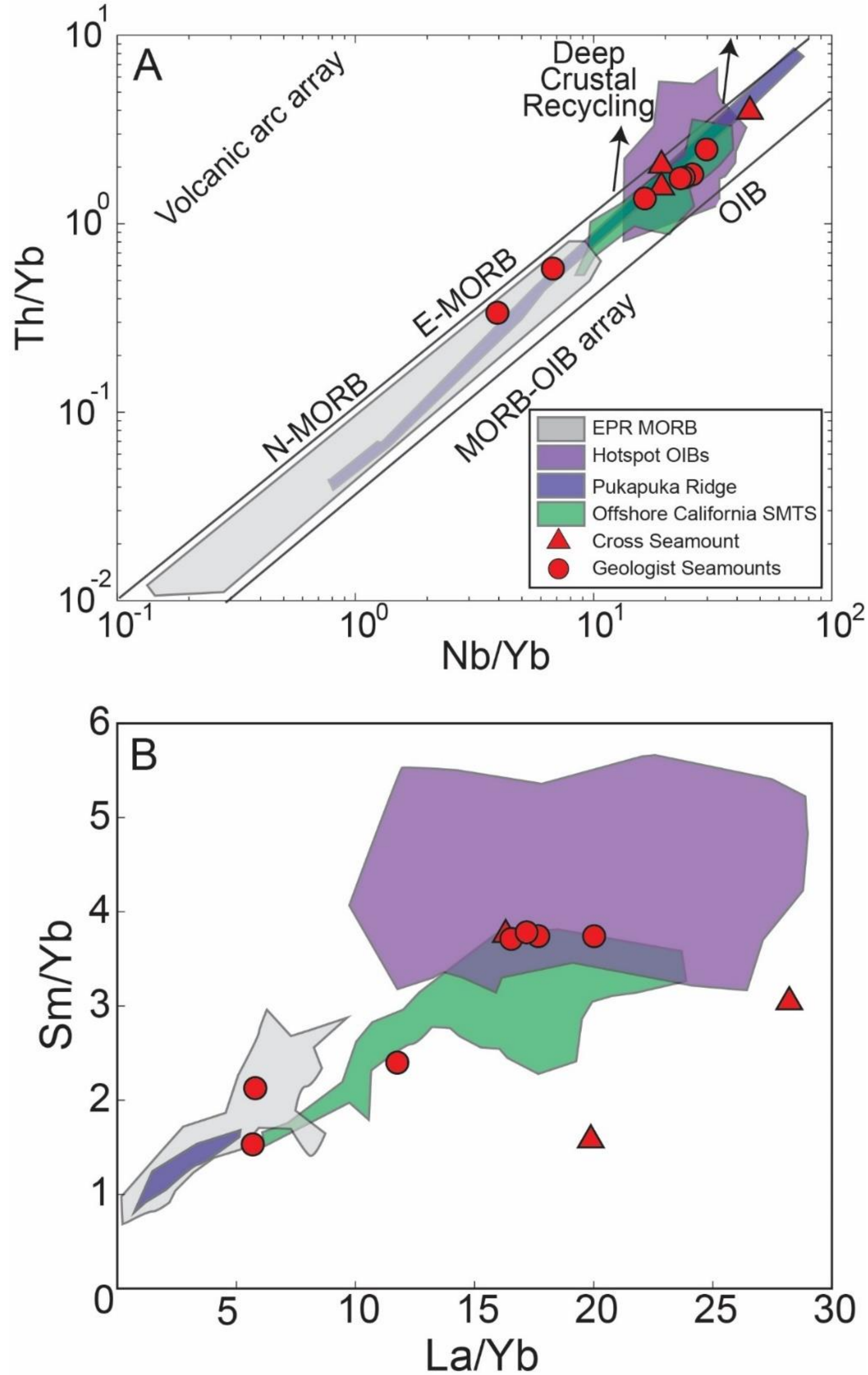

Figure 10: Key HFSE ratios for the Geologist Seamount lavas compared to relevant compositional fields. (A) Th/Yb vs. Nb/Yb diagram. The trend direction annotations and standard array fields are from Pearce (2007). (B) Sm/Yb vs. La/Yb diagram. Symbols and envelopes are the same as in Figure 7.

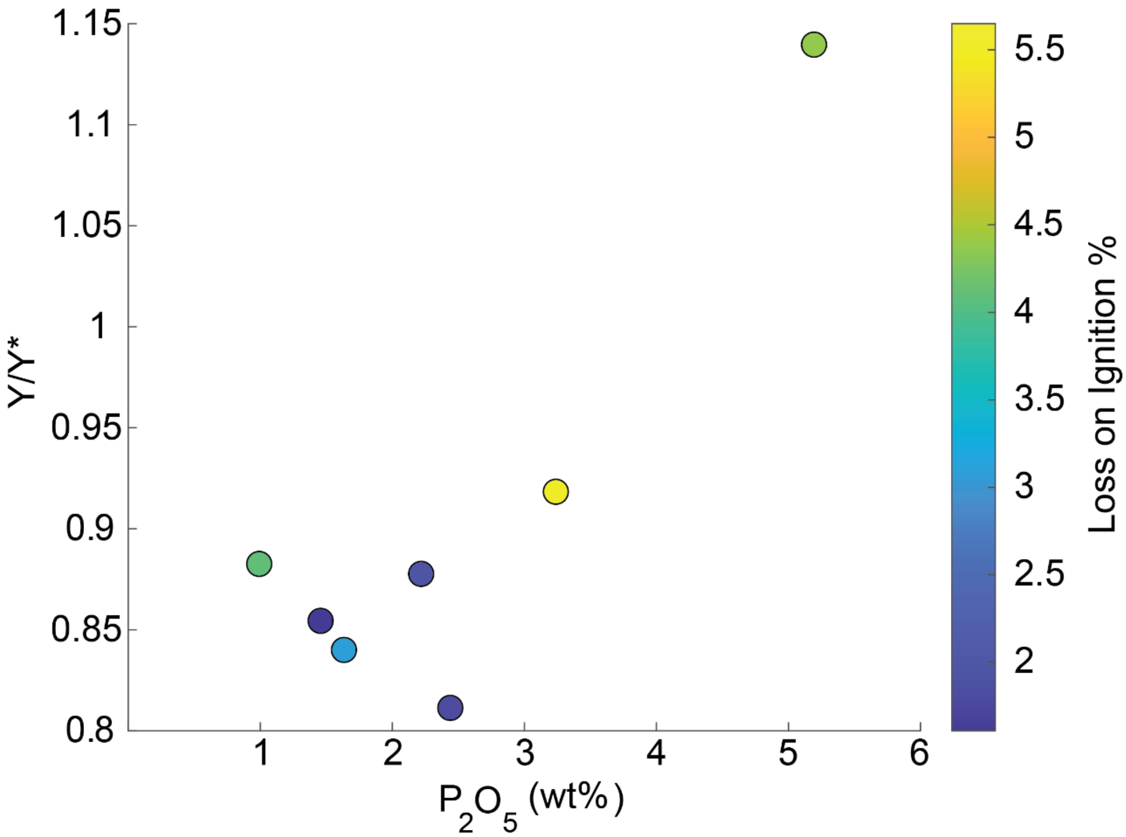

Figure 11: A plot of Y/Y* vs. P_2O_5 diagram for the Geologist seamount samples. See text for description on how these values were calculated. The circles are color-coded based on the lava flow percent LOI.

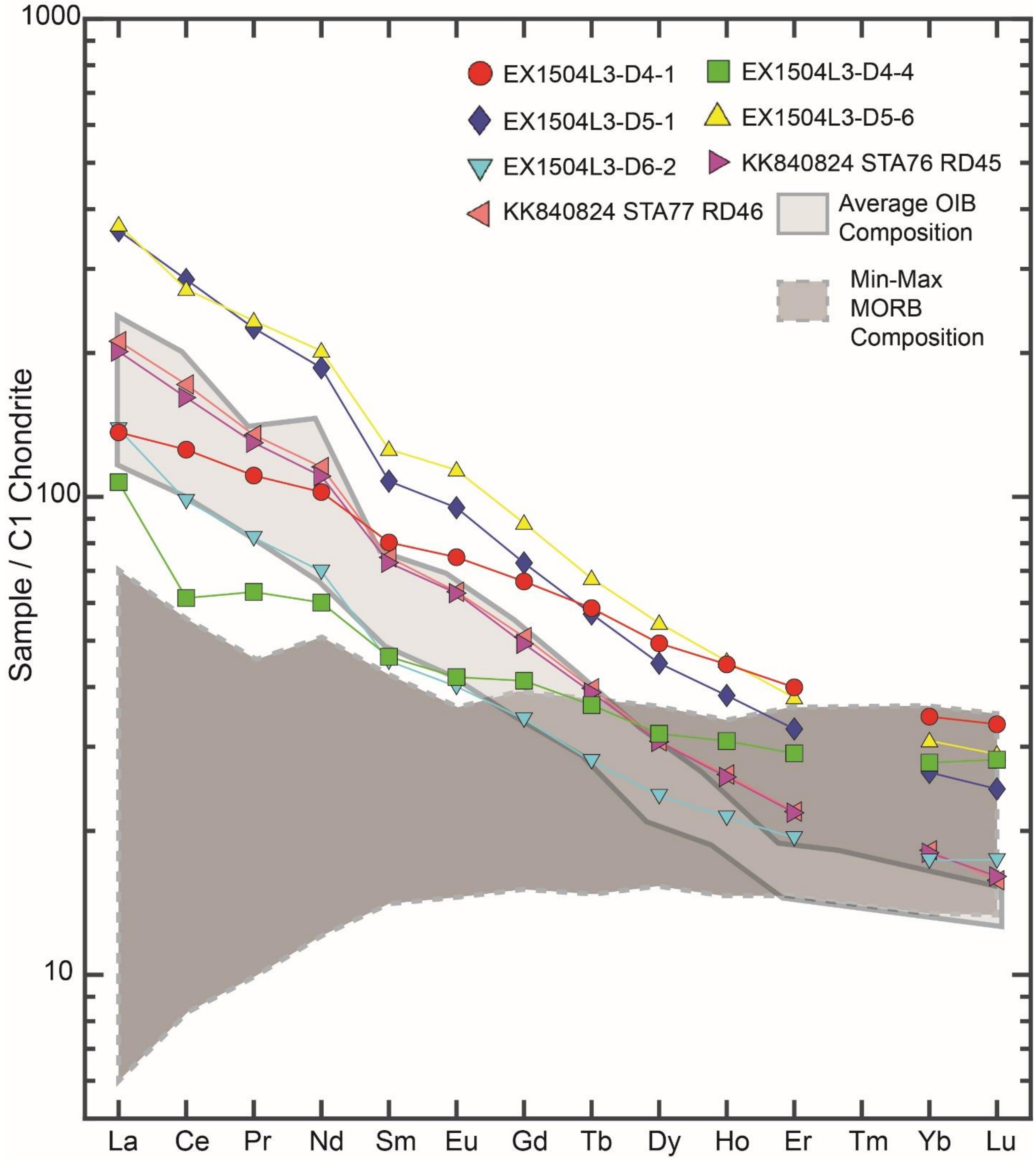

Figure 6: C1 Chondrite normalized (McDonough and Sun, 1995) rare earth element diagram displaying lava flow trends for the Geologist Seamounts, average ocean island basalt (OIB) composition, and min-max mid-ocean ridge basalt (MORB) composition. OIB dataset from Willbold and Stracke (2006), and MORB dataset from Gale et al. (2013).

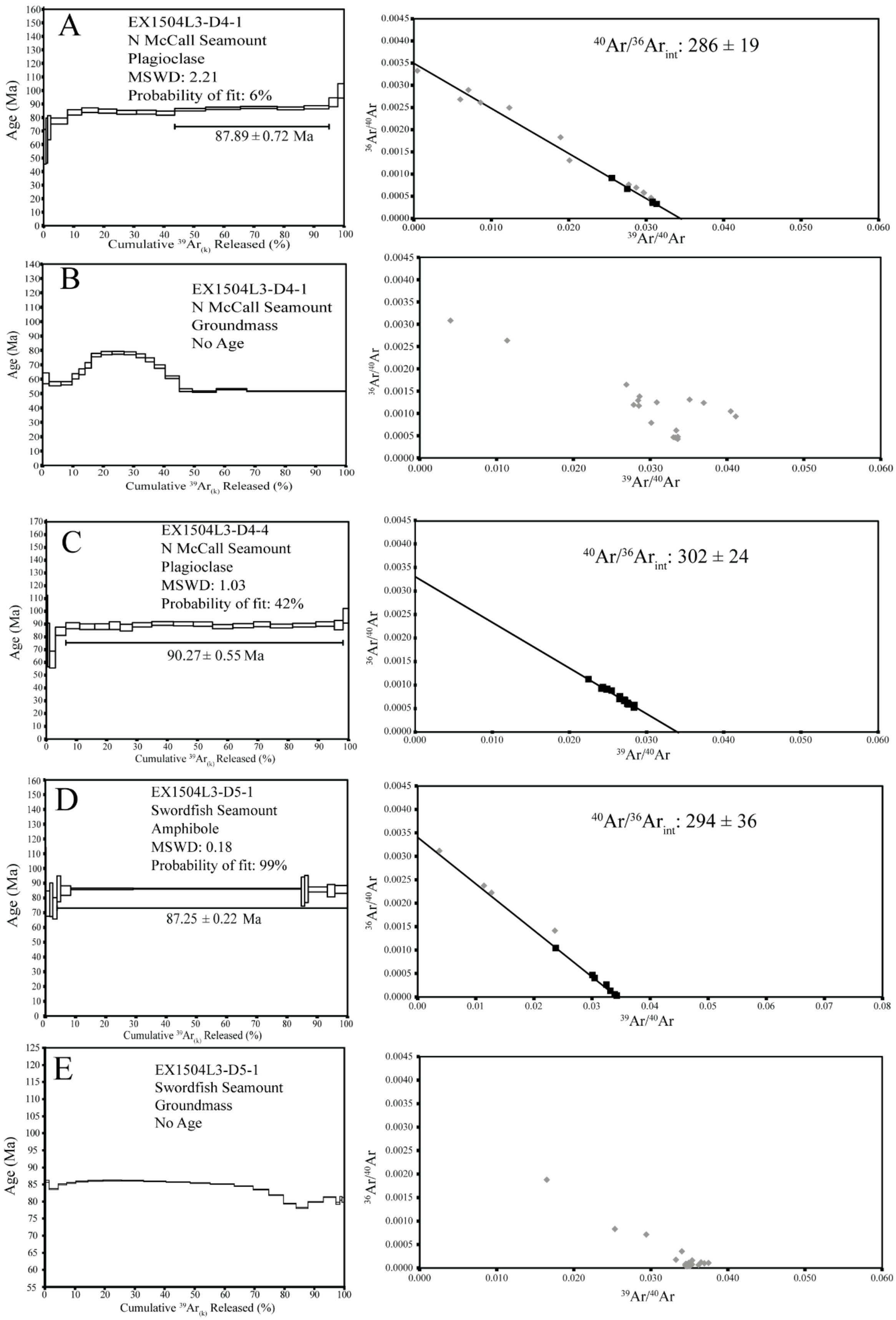
A
EX1504L3-D4-1
N McCall Seamount
Plagioclase
MSWD: 2.21
Probability of fit: 6%
87.89 ± 0.72 Ma
Age (Ma)
Cumulative 39Ar(k) Released (%)
40Ar/36Arint: 286 ± 19
36Ar/40Ar
39Ar/40Ar
B
EX1504L3-D4-1
N McCall Seamount
Groundmass
No Age
C
EX1504L3-D4-4
N McCall Seamount
Plagioclase
MSWD: 1.03
Probability of fit: 42%
90.27 ± 0.55 Ma
40Ar/36Arint: 302 ± 24
D
EX1504L3-D5-1
Swordfish Seamount
Amphibole
MSWD: 0.18
Probability of fit: 99%
87.25 ± 0.22 Ma
40Ar/36Arint: 294 ± 36
E
EX1504L3-D5-1
Swordfish Seamount
Groundmass
No Age

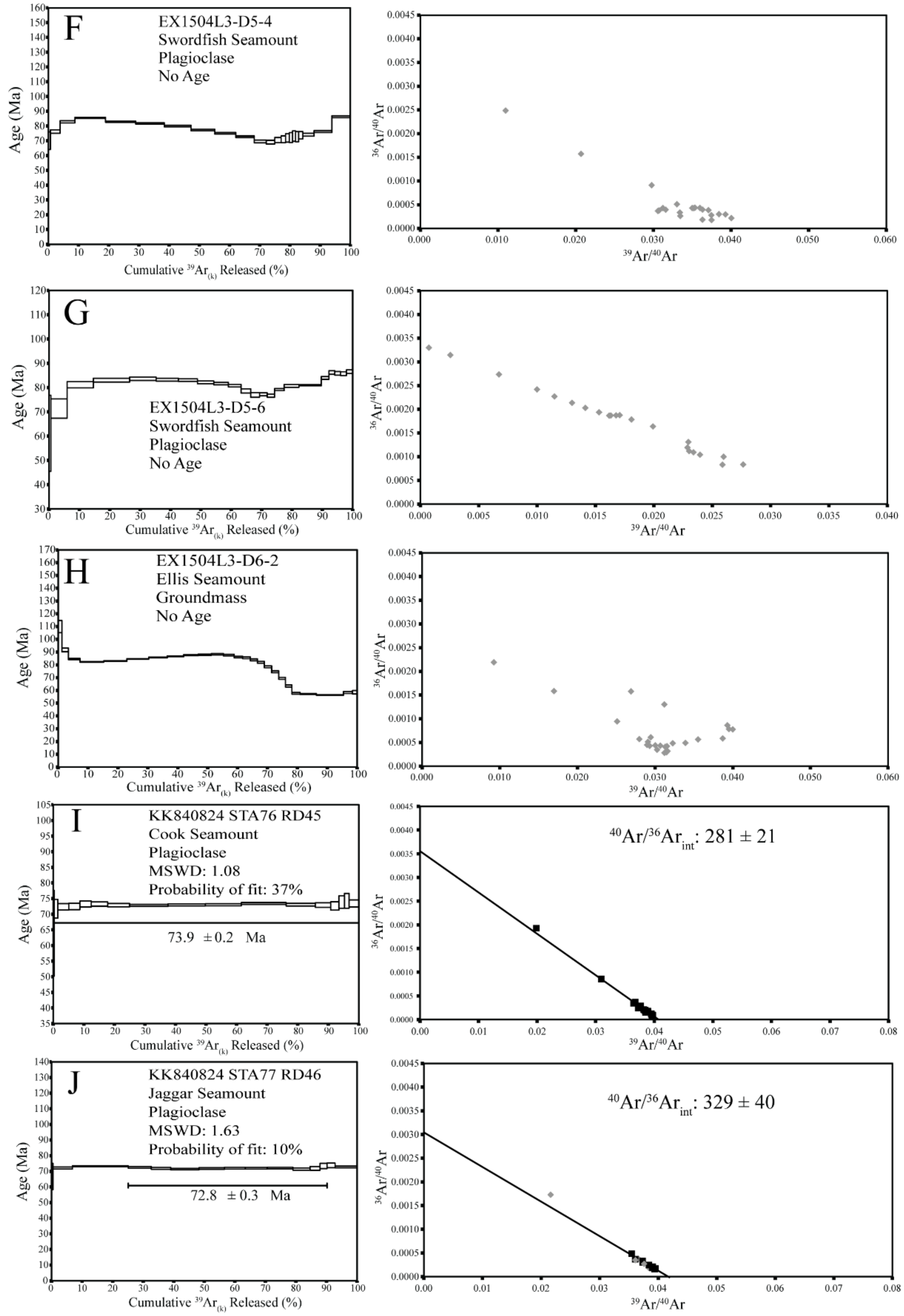

Figure 13: Incremental heating $^{40}Ar/^{39}Ar$ age determination and inverse isochron analyses for the recovered EX1504L3 and KK840824-02 lava flows. Uncertainties provided at the $\pm 2\sigma$ confidence level.

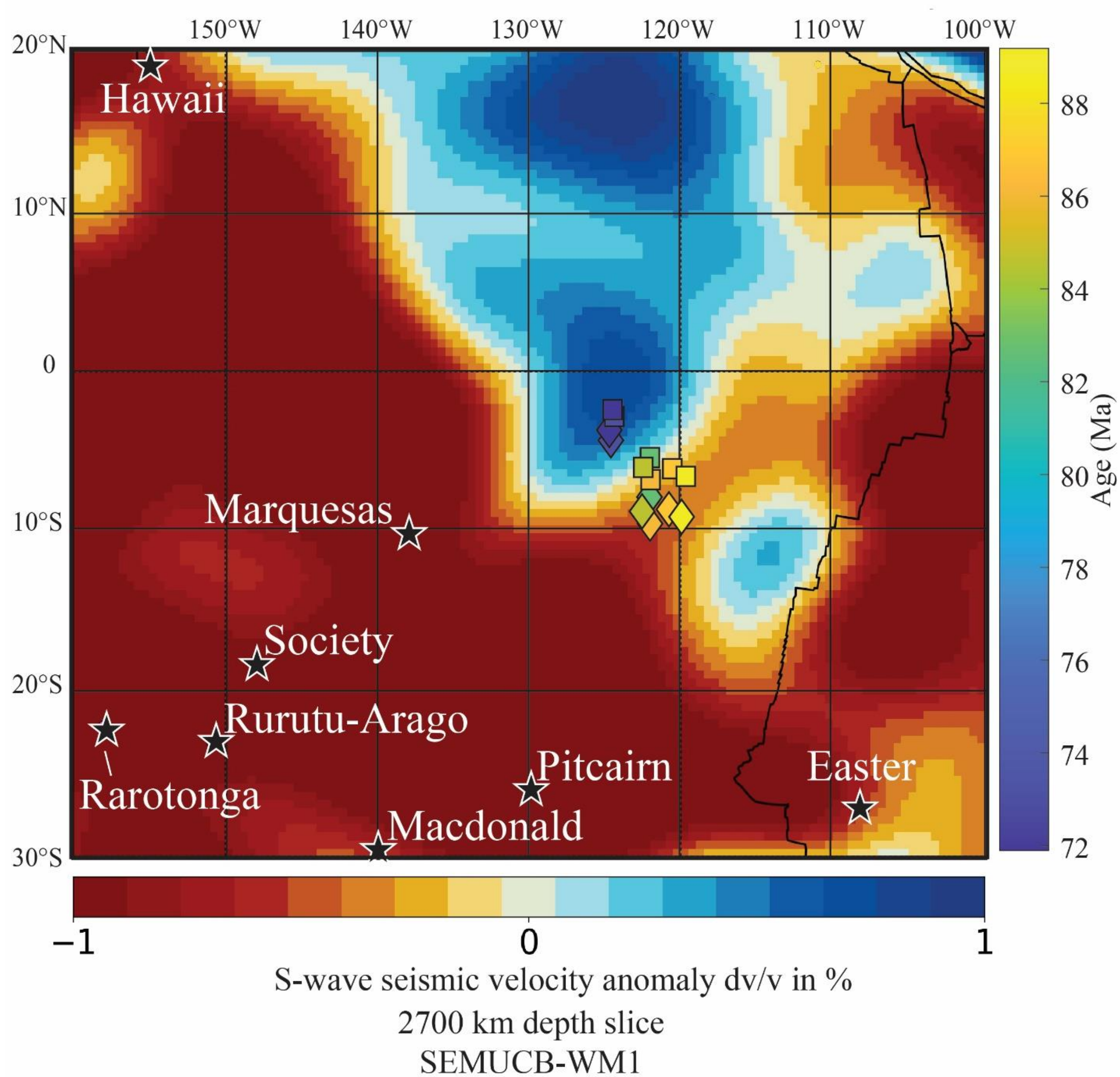

Figure 14: A map that shows the location of the where individual Geologist Seamounts lava flows (diamonds and squares) were emplaced during the late Cretaceous overlain on modern-day mantle shear-wave seismic anomaly (in %) at 2700 km depth. The seismic velocity map is calculated using the SEMUCB-WM1 model (French and Romanowicz, 2015) using the SubMachine model of Hosseini et al. (2018). Diamond seamount locations based on the fixed hotspot plate motion model from Wessel and Kroenke (2008), and square seamount locations based on the mobile hotspot plate motion model from Doubrovine et al. (2012). Black stars are present-day hotspot locations from Koppers et al. (2021). Thick solid black lines are plate boundaries, primarily the modern East Pacific Rise.

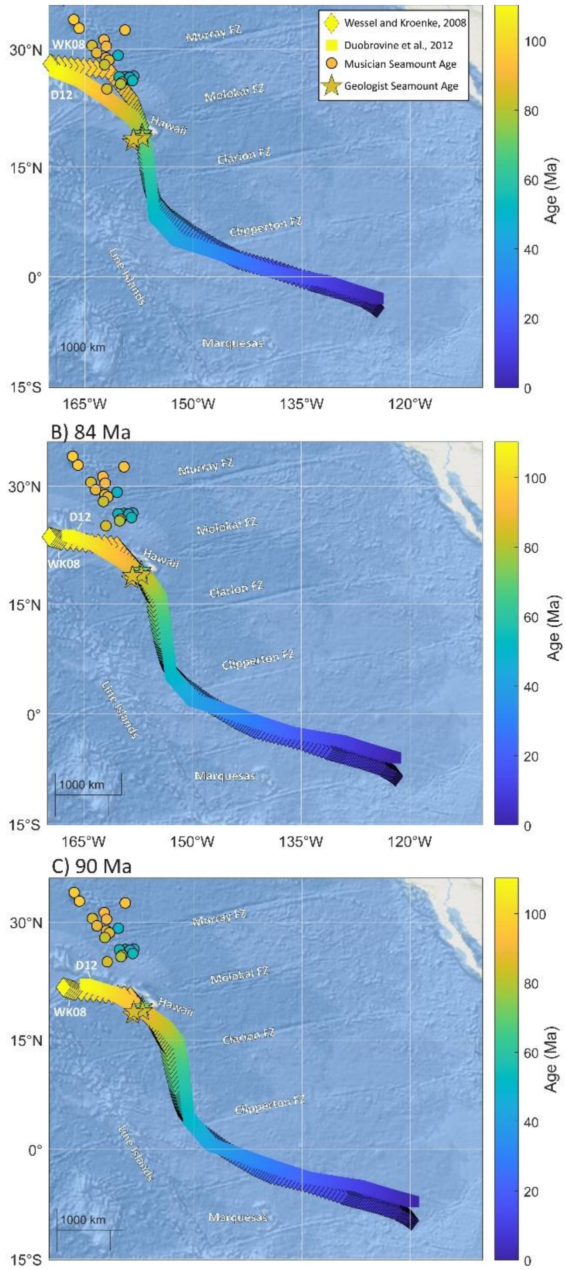

Figure 15: Maps of theoretical hotspot tracks from 110–0 Ma based on the assumption that the three volcanic episodes within the Geologist Seamounts represent the lithosphere overriding a fixed mantle plume at the time of volcanism. Diamonds are incremental hotspot locations overtime based on a fixed mantle plume model from Wessel and Kroenke (2008). Squares are incremental hotspot locations overtime based on a mobile mantle plume model from Doubrovine et al. (2012). Circles are ages of lava flows from the Musician Seamounts from Balbas et al. (2023). Stars are ages of lava flows from the Geologist Seamounts (this study and Sager and Pringle, 1987). (A) Hotspot tracks based on a 73 Ma volcanic episode within the Geologist Seamounts. The hotspot track potentially correlates with Euterpe plume (Musician Seamounts) volcanism in the WK08 model but would require extreme southward deflection of the plume. (B) Hotspot tracks based on an 84 Ma volcanic episode within the Geologist Seamounts. No correlation with any known mantle plume is observed. (C) Hotspot tracks based on an 90 Ma volcanic episode within the Geologist Seamounts. No correlation with any known mantle plume is observed.

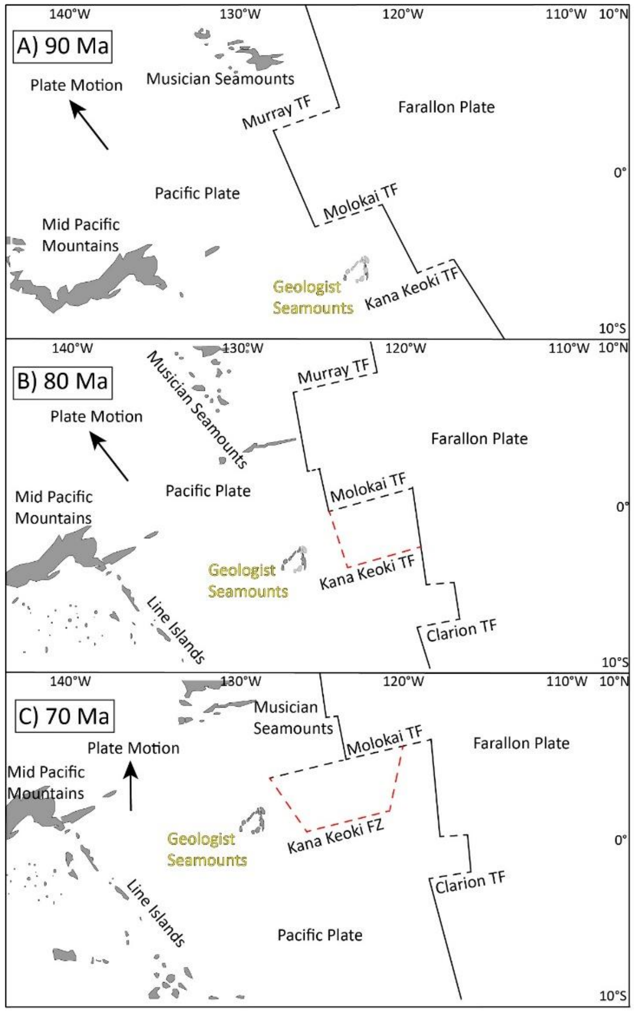

Figure 16: A schematic evolution of the Geologist Seamounts cluster over three 10 Ma time slices. The position of ridges and volcanic structures are constrained using GPlates software (Müller et al. 2018) using the plate motion model of Müller et al. (2019) and isochron reconstructions of Seton et al. (2020). Latitude and longitude labels are approximate and can vary based on plate motion model employed. Black solid lines are spreading center axes, and black dashed lines are transform fault (TF) and fracture zone (FZ) traces. Red dashed lines are schematic evolution of a proposed microplate. Grey shapes are seafloor structures proximal to the Geologist Seamounts during time slices from Johansson et al. (2018). Plate motion vectors are approximate. The Geologist Seamounts shape is maintained throughout each time slice although seamounts are made translucent if age/orientation relationship is much younger than the time slice (e.g. All seamounts except those oriented N-S and aged 90–87 Ma are translucent in the 90 Ma time slice; all seamounts except those oriented N-S or NE-SW and aged 90–87 Ma or 84 Ma are made translucent in the 80 Ma time slice; all seamounts are opaque in the 70 Ma time slice). (A) 90 Ma time slice showing initial formation of the Geologist Seamounts and its proximity to the paleo Pacific-Farallon spreading center. The Musician Seamounts (Euterpe Plume) is located distal from the Geologist Seamounts at 90 Ma. (B) 80 Ma time slice showing the schematic growth of a microplate caused by ridge-jump from plate reorganization. Its' proximity to the Geologist Seamounts is of note since volcanism occurred within the cluster at approximately 83 Ma. The Kana Keoki TF develops into an aseismic FZ during this time. (C) 70 Ma time slice showing the schematic extent of a microplate in the region, and a change in plate motion just after volcanism occurred on the Geologist Seamounts at 74–73 Ma.

Table 1: Seamount characteristics including base and peak depth, peak location, height, morphology, and primary orientation. We define a congruent base depth of 4500 mbsl for the surrounding seafloor. McCall and Pensacola seamounts are separated into different sections based on their distinct morphology. Radial seamounts have no primary orientation due to their radial nature. mbsl = meters below sea level.

Seamount	Peak Depth (mbsl)	Peak Latitude	Peak Longitude	Height (m)	Morphology	Primary Orientation
Swordfish	975	18.2774°N	158.4531°W	3525	Elongate Ridge	0°/180°
Cross	405	18.7138°N	158.2744°W	4095	Guyot	28°/208°
Washington	940	18.8659°N	157.9679°W	3560	Elongate Ridge	24°/204°
Ellis	1540	19.1830°N	157.6645°W	2960	Elongate Ridge	40°/220°
Perret	2230	19.3789°N	157.3179°W	2270	Elongate Ridge	20°/200°
Cook	1060	19.2992°N	157.1663°W	3440	Radial	N/A
Jaggar	1585	19.3645°N	156.9961°W	2915	Elliptical Elongate	335°/155°
N McCall	2560	19.0106°N	157.1105°W	1940	Elongate Ridge	0°/180°
Central McCall	930	18.7222°N	157.0755°W	3570	Elongate Ridge	20°/200°
S McCall	1250	18.5685°	157.0416°W	3250	Elongate Ridge	0°/180°
E Pensacola	650	18.2869°N	157.3323°W	3850	Radial	N/A
W Pensacola	1435	18.2114°N	157.445°W	3065	Radial	N/A
Daly	1260	18.1259°N	157.6600°W	3240	Radial	N/A

Table 2: Sample location information for eight lava flows from five seamounts within the Geologist Seamounts cluster. EX1504L3 samples were recovered by ROV Deep Discoverer in 2015. KK840824-02 samples were recovered by SOEST in 1984. The dredged depths for the KK84 samples are best estimates based on length of dredge wire and the angle of the wire relative to the ship.

Sample	Recovery Method	Seamount	Latitude (°N)	Longitude (°W)	Depth (m)
EX1504L3-D5-1	ROV	Swordfish	18.31	158.46	1071
EX1504L3-D5-4	ROV	Swordfish	18.31	158.46	969
EX1504L3-D5-6	ROV	Swordfish	18.31	158.46	973
EX1504L3-D6-2	ROV	Ellis	19.23	157.61	2125
KK840824-02 STA76 RD45	Dredge	Cook	19.24	157.17	3045
KK840824-02 STA77 RD46	Dredge	Jaggar	19.41	157.08	3000
EX1504L3-D4-1	ROV	McCall	18.98	157.11	2699
EX1504L3-D4-4	ROV	McCall	18.98	157.11	2634

Table 3: Major and trace element data for six lava flow samples recovered from the Geologist Seamounts. Major elements are reported in weight percent. LOI = Loss on Ignition. LOI calculated from analysis by measuring sample weight prior to and after the ignition process. Rock types based on normalization to 100% (classification scheme from Le Bas, 1986). TrAn = Trachyandesite. Bas = Basanite. PhTe = Phonotephrite. Haw = Hawaiite. Trace elements are reported in parts per million.

Seamount:	**Swordfish**		**Ellis**	**Cook**	**Jaggar**	**McCall**	
Sample:	**EX1504L3-D5-1**	**EX1504L3-D5-6**	**EX1504L3-D6-2**	**KK840824-02 STA76 RD45**	**KK840824-02 STA77 RD46**	**EX1504L3-D4-1**	**EX1504L3-D4-4**
Rock type:	TrAn	TrAn	Bas	Bas	PhTe	Haw	Bas
(wt.%)							
SiO_2	54.9	53.5	42.6	46.4	48.9	47.6	43.1
TiO_2	1.6	3.0	2.4	3.0	2.7	2.5	2.6
Al_2O_3	18.6	19.5	17.5	18.2	18.2	19.7	17.1
Fe_2O_3	3.5	5.2	12.2	11.2	8.6	11.3	8.7
MnO	0.06	0.05	0.19	0.14	0.10	0.14	0.11
MgO	0.40	0.50	1.3	1.4	1.1	1.1	1.2
CaO	6.9	5.9	9.9	8.4	8.2	6.9	12.4
Na_2O	5.4	4.5	3.1	4.3	4.4	4.3	3.6
K_2O	4.2	4.5	1.9	2.1	3.3	1.0	1.6
P_2O_5	2.4	1.4	3.0	1.6	2.2	0.95	4.9
LOI	1.8	1.6	5.6	3.1	1.9	4.1	4.4
Total	97.9	98.1	94.2	96.7	97.8	95.8	95.5
(ppm)							
Sc	8.96	24.23	26.10	16.06	14.53	24.02	15.56
V	65.01	278.7	300.5	207.3	183.5	370.4	130.1
Cr	3.33	25.18	243.3	70.55	46.45	89.32	41.63
Co	4.98	16.26	42.47	34.42	19.50	51.09	15.13
Ni	4.801	18.36	86.81	56.23	33.09	69.73	34.31
Ga	35.34	44.24	20.04	27.85	27.64	41.06	20.11
Rb	97.93	116.2	32.31	31.64	55.14	22.91	18.62
Sr	1136	1487	559.5	894.2	853.0	571.0	362.1
Y	52.95	66.72	32.49	37.28	39.24	65.15	56.26
Zr	575.8	628.5	240.5	351.3	370.6	503.2	203.1
Nb	126.9	129.0	45.85	66.46	69.63	37.67	17.65
Cs	0.20	0.61	1.14	0.37	1.16	0.90	0.66
Ba	1122	1125	311.3	414.1	413.0	152.3	71.42
La	85.43	87.86	32.87	47.72	50.15	32.34	25.44
Ce	174.6	166.7	60.18	98.90	105.3	76.95	37.64
Pr	20.92	21.67	7.620	12.04	12.51	10.28	5.87
Nd	85.11	92.30	31.93	50.49	52.78	46.78	27.46
Sm	15.97	18.60	6.708	10.77	11.06	11.88	6.85
Eu	5.34	6.41	2.26	3.54	3.56	4.21	2.36
Gd	14.47	17.53	6.82	9.80	10.13	13.24	8.20

Tb	2.05	2.44	1.01	1.41	1.44	2.11	1.32
Dy	11.03	13.38	5.83	7.56	7.58	12.15	7.86
Ho	2.10	2.47	1.17	1.42	1.43	2.44	1.68
Er	5.22	6.08	3.10	3.49	3.51	6.39	4.65
Yb	4.27	4.97	2.80	2.90	2.9	5.58	4.47
Lu	0.60	0.71	0.43	0.39	0.39	0.82	0.69
Hf	15.79	14.95	6.02	8.38	8.43	12.38	5.92
Ta	8.59	8.12	2.90	3.76	3.72	2.34	1.20
Pb	6.68	4.96	5.12	3.18	3.65	4.13	1.99
Th	10.59	9.09	3.81	4.94	5.05	3.23	1.51
U	1.84	3.19	1.56	1.17	2.34	1.20	1.28

Table 4: Incremental heating $^{40}Ar/^{39}Ar$ age determination analyses data for the recovered EX1504L3 and KK840824-02 lava flows. Total fusion age given for discordant analyses. ^{39}Ar is the cumulative concentration of $^{39}Ar_K$ gas included in plateau calculation. A plateau is defined as having >50% of ^{39}Ar and >5% P. P = Probability of fit. MSWD = Mean Square of Weighted Deviates. Pl = Plagioclase, GM = Groundmass, Amph = Amphibole. Uncertainties provided at the ±2σ confidence level.

Seamount	Sample	Phase	Size (μm)	Plateau age (Ma)	^{39}Ar %	MSWD	P %	$^{40}Ar/^{39}Ar$ intercept	Inverse isochron age (Ma)
McCall	EX1504L3-D4-1	Plag	250–500	87.9 ± 0.7	51	2.22	6	286 ± 19	88.6 ± 1.2
McCall	EX1504L3-D4-1	GM	212–300						
McCall	EX1504L3-D4-4	Plag	250–500	90.3 ± 0.6	92	1.03	42	302 ± 24	90.0 ± 2.0
Swordfish	EX1504L3-D5-1	Amph	250–500	87.3 ± 0.2	96	0.18	99	294 ± 36	87.3 ± 0.4
Swordfish	EX1504L3-D5-1	GM	212–300						
Swordfish	EX1504L3-D5-4	Plag	250–500						
Swordfish	EX1504L3-D5-6	Plag	250–500						
Ellis	EX1504L3-D6-2	GM	212–300						
Cook	KK840824-02 STA76 RD45	Plag	250–500	73.9 ± 0.2	100	1.08	37	281 ± 21	74.2± 0.2
Jaggar	KK840824-02 STA76 RD46	Plag	250–500	72.8 ± 0.3	65	1.63	10	329 ± 37	72.3 ± 0.7